Geophys. J. Int. (1996) **126**, 712–734

Progressive growth of San Clemente Island, California, by blind thrust faulting: implications for fault slip partitioning in the California Continental Borderland

Steven N. Ward[1] and Gianluca Valensise[2]

[1] *Institute of Tectonics, University of California, Santa Cruz, CA 95064, USA*
[2] *Istituto Nazionale di Geofisica, Via di Vigna Murata 605, 00143 Rome, Italy*

Accepted 1996 March 31. Received 1996 March 6; in original form 1995 October 16

SUMMARY

We find that the genesis of San Clemente Island and its surrounding submarine platform is consistent with progressive slip on two, southeast-striking, southwest-dipping, blind thrust fault segments. Since their inception 2 to 5 Ma, 3 km of compression normal to the N150°E fault strike has been accommodated with 1700 m of domal uplift of the San Clemente Anticlinorium. The existence of an extensive suite of Pleistocene marine terraces provides evidence that slip and uplift are continuing today. Based on direct terrace fossil age determinations and correlations of terrace heights with global sea-level curves, we estimate that San Clemente Island is currently uplifting at between 0.2 and 0.5 mm yr^{-1}. This translates into 0.6–1.5 mm yr^{-1} of thrusting on the causative blind thrusts beneath the island. Unlike the situation at nearby Palos Verdes, where a simple twist in a regional strike-slip fault accommodated both fault-parallel and fault-normal motions, the shallow dips of the thrusts suggest that, if regional strike-slip motion on the San Clemente Fault exists, it must be partitioned onto through-going surfaces distinct from the thrusts. Current GPS data are sparse and equivocal, but they indicate that 1–4 mm yr^{-1} of compression and 4–7 mm yr^{-1} of strike slip are absorbed in the California Continental Borderland. With the Palos Verdes Fault taking some 3 mm yr^{-1} from the strike-slip budget, 1–4 mm yr^{-1} of motion could be present on a through-going San Clemente Fault. When translated into an annual moment release rate using Kostrov's formula, GPS strains predict that between 2.5 and 4.9 $\times 10^{17}$ N m yr^{-1} of earthquake potential is available offshore from San Diego to the Santa Barbara Channel. Distribution of this moment budget among various earthquake magnitudes is arguable, but we predict that $M > 6$ quakes in the Borderland could recur between 30 and 80 years, and $M > 7$ quakes might be found every 310 to 580 years.

Key words: California Continental Borderland, fault tectonics, San Clemente Island.

1 INTRODUCTION

San Clemente Island off the southern California coast (Fig. 1) was first charted in 1602 by Spanish explorer Sebastian Vizcaino, who named the place after a patron whose feast day had been celebrated two days before the Island's discovery. San Clemente is the southernmost of the Channel Islands belonging to the California Continental Borderland, a vast, mostly submarine, region bounded by the Santa Barbara Channel to the north, the Patton escarpment to the west, the present coastline to the east and the Bahia Sebastian Vizcaino, a broad westward projection of Baja California, to the south. The California Continental Borderland is a vigorous and complex component of the Pacific–North America plate boundary that has experienced subduction, rifting and transform faulting in the relatively short interval between the Oligocene (36 Ma) and the present. Over time, geometrical irregularities of the plate boundary have forced large crustal blocks to rotate, producing both contraction and extension within postulated microplates caught between the Pacific and North American plates proper (Legg 1991; Legg & Kennedy 1991).

Although the California Continental Borderland is an active part of a plate boundary, the complexity of its geodynamic evolution and the difficulties involved in collecting submarine geological data have limited the resolution of its tectonic traits

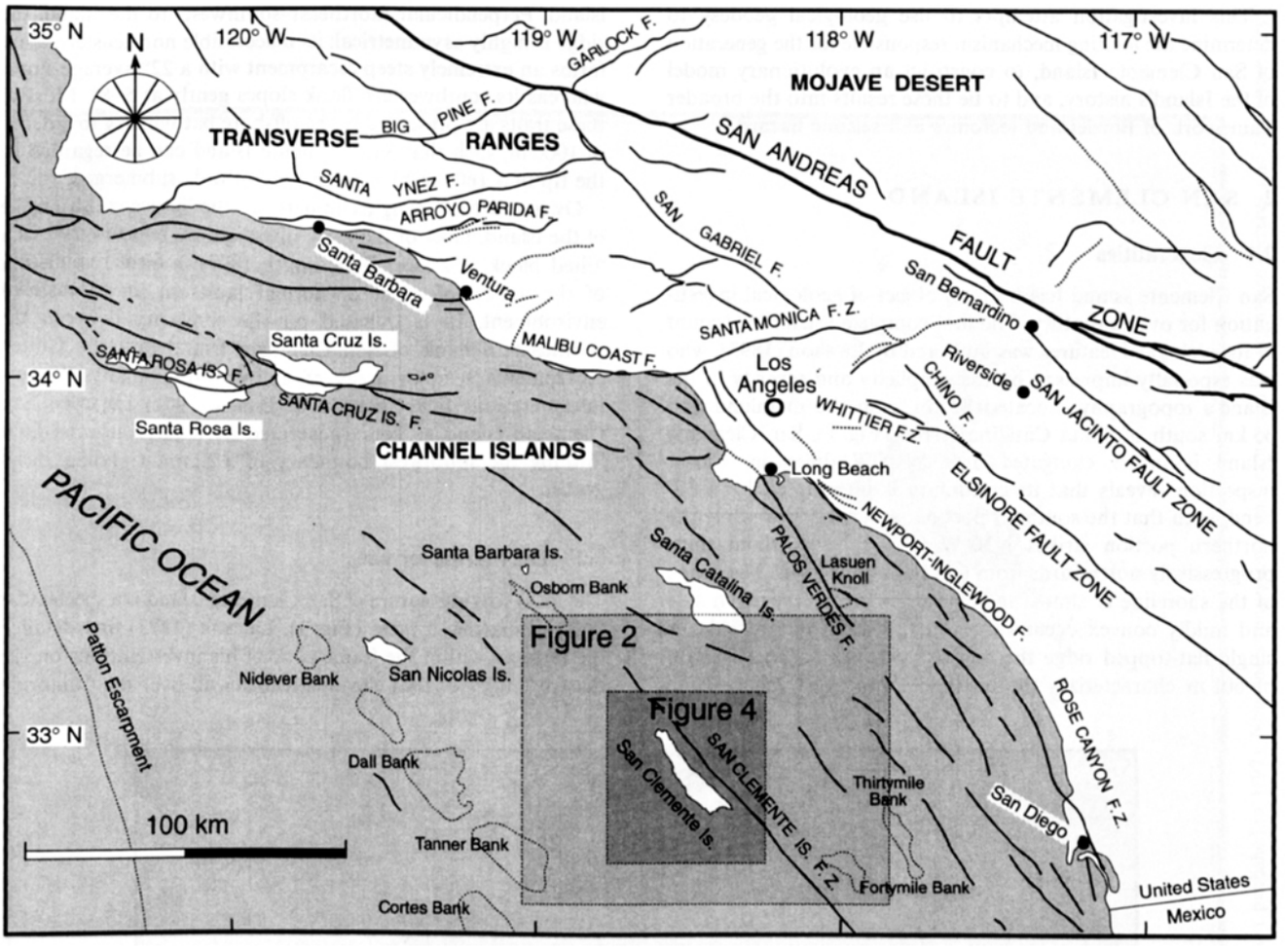

Figure 1. Map view of the southern California Continental Borderland. The Borderland contains many faults and compressive geological structures that accommodate both compressional and strike-slip components of Pacific–North America plate motion. The specific modes of deformation within the Borderland, however, are not well understood, nor is the region's level of seismic hazard.

even to the extent of conclusively establishing the fraction of Pacific–North American plate motion accommodated across it. Models developed in the late 1970s suggested that by Late Miocene time (about 10 Ma) most relative plate motion had been transferred eastwards onto the San Andreas transform fault system, and that activity of offshore faults was subsequently slight (Blake *et al.* 1978; Crowell 1979; Crouch 1981). By the beginning of the 1980s, new estimates of the total slip budget of the major onshore faults of southern California pointed to a deficit with respect to the predicted Pacific–North American plate rate, and inference rose that coastal or offshore faults of the California Continental Borderland actually may be absorbing as much as one-third of the relative motion (Anderson 1979; Weldon & Humphreys 1986; Minster & Jordan 1987). Although the magnitude of this 'San Andreas discrepancy' has since been lowered by revisions in global plate-motion models (Demets *et al.* 1990), geodetic data (Ward 1990; Feigl *et al.* 1993) continue to indicate that substantial secular straining persists offshore. The mechanism by which these strains are accommodated tectonically is uncertain; however, the concentration of background seismicity within the California Continental Borderland along rectilinear trends suggests that offshore deformation is probably localized onto a limited number of major structures in a style similar to that presented onshore by the Elsinore and San Jacinto Faults. Although the geodetic sites are too sparse to resolve individually these offshore faults, evidence indicates that action on such faults has in fact generated the islands upon which the geodetic sites sit. Potentially, the styles and slip rates of these poorly understood offshore faults could thus be revealed by interpreting the patterns of cumulated deformation recorded by geological topographic and geomorphological features on the various Channel Islands.

'Geological Geodesy' of this type has already successfully inferred the style and rate of the seismically quiescent, blind central Palos Verdes Fault, at the eastern edge of the California Continental Borderland (Ward & Valensise 1994). The growth of the Palos Verdes Hills was found to be a mechanical consequence of 3 mm yr^{-1} slip along a 30 km long restraining bend on the right-lateral Palos Verdes Fault. [This rate was later confirmed by McNeilan, Rockwell & Resnick (1996) for the offshore section of the fault south of Long Beach.] Neighbouring San Clemente Island bears some resemblance to the Palos Verdes Hills, and might be an offshore analogue. Thus, information pertinent to the San Clemente Fault may derive from similar analysis.

This investigation attempts to use geological geodesy to determine the faulting mechanism responsible for the generation of San Clemente Island, to construct an evolutionary model of the Island's history, and to tie these results into the broader framework of Borderland tectonics and seismic hazard.

2 SAN CLEMENTE ISLAND

2.1 Generalities

San Clemente Island has been an object of geological investigation for over a century. The first complete scientific account of its geological features was authored by Lawson (1893), who was especially impressed by the simplicity and severity of the island's topography. Located 80 km from the mainland and 35 km south of Santa Catalina Island (Fig. 1), San Clemente Island is rather elongated in a N40°W direction. Closer inspection reveals that its continuity is interrupted by a 20° bend, such that the southern portion strikes N50°W while the northern portion strikes N30°W (Fig. 2). The island thins progressively northwards from 6 km to about 2 km. The shape of the shoreline is almost rectilinear on the northeastern side and mildly convex oceanwards on the southwestern side. A single flat-topped ridge that slowly increases to an elevation of 601 m characterizes the northwest–southeast relief of the island. Perpendicular (northeast–southwest) to the island, the ridge is highly asymmetrical: its inaccessible northeastern flank forms an extremely steep escarpment with a 22° average slope, whereas its southwestern flank slopes gently at 5–8°. Most of these traits are preserved in the offshore bathymetry to a depth of 1000 m, such that San Clemente Island can be regarded as the tip of a 1600 m high iceberg two-thirds submerged.

Owing to the strong asymmetry in the across-width profile of the island, most of the early investigators referred to it as a 'tilted block' (Lawson 1893; Smith 1897), a term reminiscent of the action of a set of normal faults in an extensional environment. In fact, based on the similarity between the northeastern flank of San Clemente Island and the faulted escarpments seen in areas of active rifting, many classical interpretations (e.g. Shepard & Emery 1941) regarded San Clemente Island as being generated by a large normal fault forming the southwest boundary of a Santa Catalina Basin graben.

2.2 The marine terraces

The most striking feature of San Clemente Island is a spectacular flight of marine terraces (Fig. 3). Lawson (1893) first detailed the terraces within the framework of his investigations on the diastrophic event that elevated features all over the California

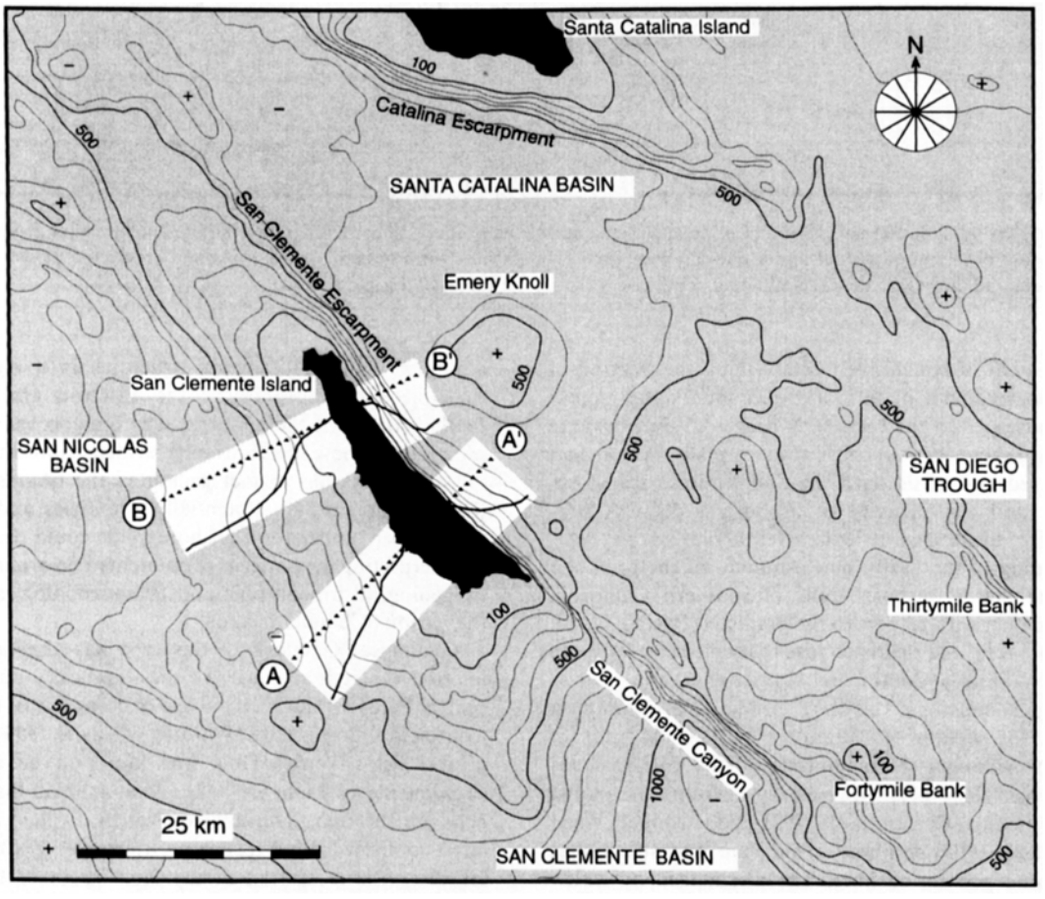

Figure 2. View of the San Clemente Island region with bathymetry contoured at 100 fathom (183 m) intervals and two sections across the island. The base sea-floor depth here is 1000–1100 m. Note the greater steepness of the island's topography/bathymetry towards the northeast versus the southwest. Although the San Clemente Island Fault is proposed to follow the San Clemente Escarpment and San Clemente Canyon, little is known about its style and slip rate.

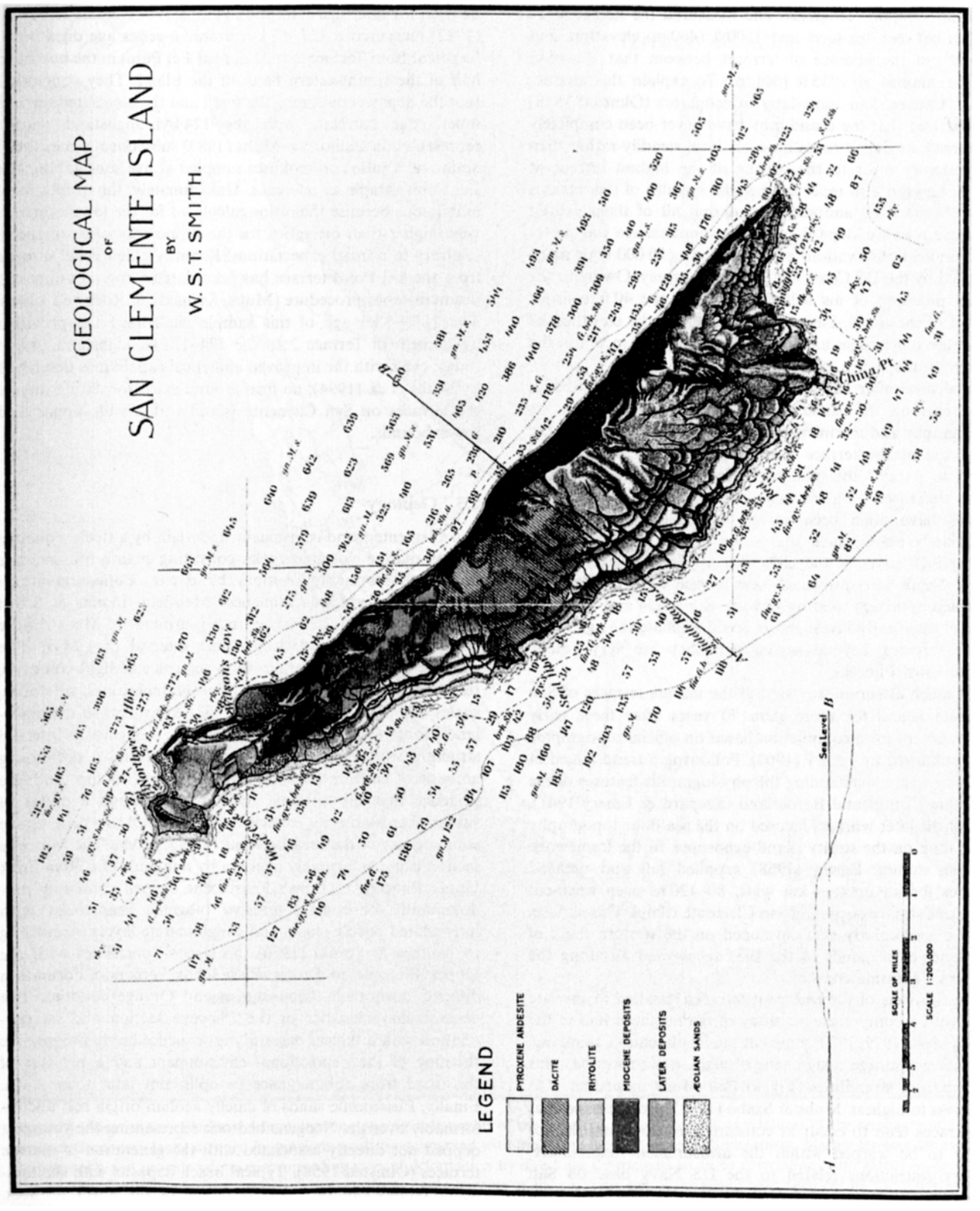

Figure 3. Geological map of San Clemente Island by W. S. T. Smith (USGS Annual report published in 1897). Note the strong geomorphic expression of the marine terraces and the asymmetry of the island's section.

coast. He concluded that the San Clemente terraces were the most spectacular in California, and that their incredible state of preservation makes them appear as if they evolved on a 'planet that had been stripped of its atmosphere, where erosion is not...'. Lawson recognized and measured the height of 22 surfaces between sea-level and 1500 ft (460 m) elevation, and pointed out the absence of terraces between that elevation and the summit at 1965 ft (601 m). To explain this characteristic, Lawson and some later investigators (Olmsted 1958) hypothesized that the island may have never been completely submerged, or that it rose above sea-level steadily rather than intermittently prior to the cutting of the highest terrace at 1500 ft. Lawson also reported that the breadth of the terraces ranges between 60 and 450 m, and that all of them exhibit low-angle seaward slope. Lawson's reconnaissance was partly based on field observations and partly on 1 : 10 000 scale maps compiled by the US Coast and Geodetic Survey. Owing to the limited precision of his field aneroid and the 40 ft contour interval of the maps, Lawson's estimates for the elevation of the terrace inner edges are accurate within 10–15 m, about the same vertical spacing as the terraces.

A few years after Lawson's work, Smith (1897) published a vast report on the island's characteristics, starting with its physiography and marine terraces (Fig. 3). Smith traced in the field some of the terrace inner edges, noting that they all tended to parallel the modern shoreline but that their continuity decreased with increasing elevation. He noticed that terraces have often been carved at the expense of those immediately above, such that some of the terraces will be missing and some of the cliffs will appear correspondingly higher. Smith also produced new terrace elevations by the combined approach used by Lawson (see Fig. 4 and Table 1). None of these early investigators could estimate the age of the marine terraces, beyond saying that they are very young, certainly post-Pliocene.

Not much attention was paid to the marine terraces of San Clemente Island for more than 70 years after these early studies, except for a compilation based on official topographic maps published by Emery (1960). Following a trend aimed at exploring and understanding the physiographic features of the California Continental Borderland (Shepard & Emery 1941), most of the later workers focused on the sea-floor topography rather than on the scanty island exposures. In the framework of these studies, Emery (1958) supplied full and detailed evidence for an up to 4 km wide, 80–120 m deep wave-cut submarine surface encircling San Clemente Island. This surface, which is particularly well developed on the western flank of the island, corresponds to the shelf recognized all along the southern California coast.

Investigations of the emergent terraces resumed in the late 1970s with a comprehensive study of the northern half of the island (Muhs 1979, 1980) aimed at the identification, mapping, correlation and age assignment of eight well-expressed, plus two subdued, strandlines (Fig. 4) that Muhs numbered 1 to 10, lowest to highest. Muhs & Szabo (1982) also observed that the terraces tend to occur at constant elevations and do not appear to be warped within the measurement uncertainty. Military restrictions related to the US Navy base on San Clemente Island prevented further investigations, and, as a consequence, no strandline mapping exists to date in the middle and southern section of the island where the highest and best-expressed terraces are to be found.

Dating of the San Clemente Island terrace sequence has not been easy nor unambiguous. Palaeontological dating failed because all of the fossil species unearthed in the terrace deposits existed from Pleistocene to the present and hence could not be used for finer age resolution (Lipps 1967). Muhs & Szabo (1982) measured a 127 ± 7 kyr uranium-series age on a coral fragment from Terrace 2 at 32 m near Eel Point in the northern half of the southwestern flank of the island. They concluded that the deposit containing the fossil and the associated terrace inner edge correlate with the 124 kyr highstand widely represented in California. Muhs (1983) subsequently measured amino-acid ratios on molluscs sampled at five sites, taking the Eel Point sample as reference. Unfortunately, the results were ambiguous because the ratios calculated for the lowest terrace were higher than the ratios for the supposedly older terraces, contrary to normal expectations. Recently a new coral sample from the Eel Point terrace has been dated using an improved uranium-series procedure (Muhs, Kennedy & Rockwell 1994). The 111 ± 3 ka age of this sample challenged the previous assignment of Terrace 2 to the 124–127 ka highstand. As of today, even with the improved analytical capabilities described by Muhs *et al.* (1994), no firm ground exists for dating any of the terraces on San Clemente Island within wide upper and lower bounds.

2.3 Geology

San Clemente Isand is primarily underlain by a thick sequence of non-marine volcanic rocks consisting mainly of andesite flows unconformably overlain by dacite. Potassium–argon dating of the volcanic sequence (Merifield, Lamar & Stout 1971) shows that it was extruded around 15 Ma (Middle Miocene) within a relatively short interval of 1 Myr. The volcanic bedrock is overlain by a sequence of light-coloured, thin-bedded Middle to Upper Miocene limestones, siltstones, shales and diatomites (Olmsted 1958) equivalent to the mainland Monterey Formation. The age of the sequence, its internal structure with volcanic sands at the base and a decreasing amount of calcium carbonate from bottom to top, and the evidence that the volcanic rocks went through a phase of subaerial erosion prior to their burial, all point to a progressive submergence of the area between 15 and 10 Ma. The Miocene section is unconformably overlain by remnants of a 30 m thick Upper Pliocene to Lower Pleistocene deposit consisting predominantly of coarse, massive biogenic sandstones with intercalated pebble lenses and conglomerate layers. According to Stadum & Susuki (1976) this deposit correlates with the Upper Pliocene to Lower Pleistocene Fernando Formation diffused onshore in Los Angeles and Orange counties. The general characteristics of the Pliocene section and its correlation with a typical basin-filling sequence imply progressive shoaling of the depositional environment and a reversal of the trend from submergence to uplift not later than 3 Ma. Finally, Pleistocene sands of chiefly aeolian origin rest unconformably over the Neogene bedrock representing the youngest deposit not directly associated with the generation of marine terraces (Olmsted 1958). Typical beach deposits with shallow-water faunas can be found on some of the lower terraces. These deposits are frequently capped by alluvial fans up to 10 m thick, particularly at the mouth of the main southwest-draining canyons.

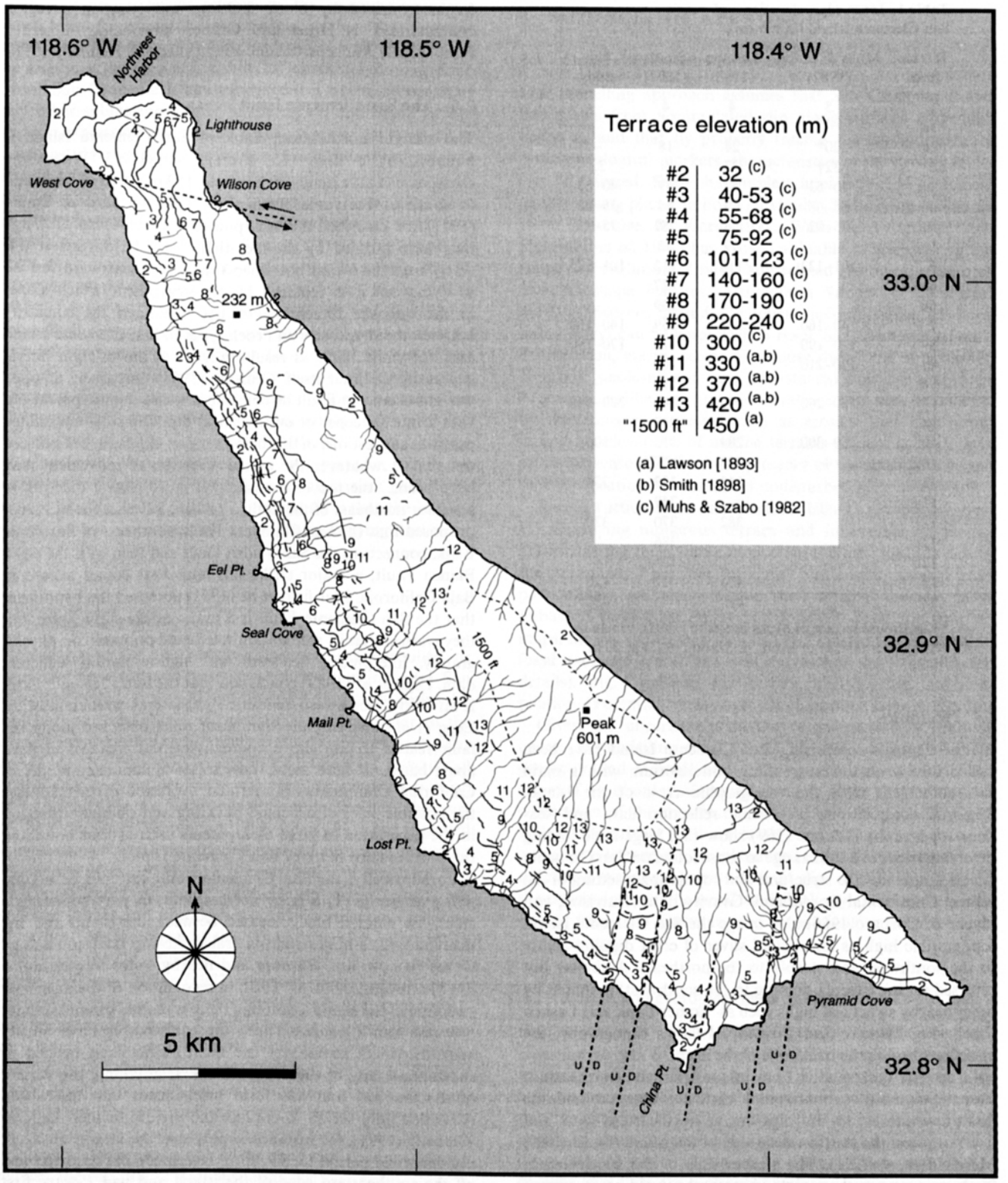

Figure 4. View of San Clemente Island showing our reconstruction of the locations, elevations and correlations of the remnants of 13 marine terraces. Secondary faults mapped by previous workers are marked with their hypothesized sense of displacement. Marine terraces are evidence of current uplift and provide information regarding rates of deformation by direct age determinations or by correlations with global sea-level curves. The terrace distribution is fairly orderly; however, the younger terraces at the southern end of the island have been cut by the action of shallow north–south-trending normal faults.

Table 1. Inner-edge elevations of marine terraces on San Clemente Island (in metres).

Terrace level	Muhs & Szabo (1982)	Lawson (1983)	Smith (1897)	This study
1	5	4	4	–
1a	–	12	–	–
1c	20*	24	18	–
2	32†	37	–	32
3	40–53	52	47	40–53
4	55–68	69	64	55–68
5	75–92	86	78?	75–92
5a	–	99	92	–
6	101–123	116	112	101–123
6a	–	–	127	–
6b	–	144	139	–
7	140–160	168	159	140–160
8	170–190	177	176	170–190
8a	190–210	–	200	–
8b	–	–	219	–
9	220–240	240	240	220–240
9a	–	–	260	–
10	250–300	284	275	300
10a	–	293	298?	–
11	–	318	333	330
11a	–	–	349	–
12	–	382	370	370
12a	–	–	386	–
12b	–	–	405	–
13	–	420	417	420
14	–	458	–	450

* Lighthouse terrace of Muhs & Szabo (1982); † includes NOTS Pier terrace of Muhs & Szabo (1982) at 30 m.

2.4 Tectonics

All the deposits comprising San Clemente Island have been folded into a northwest-trending anticlinorium with a main axis coincident with the topographic crest of the island. Regional compilations of seismic reflection data and sea-floor topography (Moore 1969) show that large-scale folding involving rocks of a similar age to those found on San Clemente Island dominates the structural and topographic setting of the central Continental Borderland. Gravity data (Harrison, von Huene & Corbarò 1966) also image the San Clemente Island topographic high as an uplifted sliver of crust dipping gently to the southwest and steeply to the northeast. A similar but reversed setting (steeply dipping to the southwest) is shared by other nearby structural highs such as Tanner Bank and Lasuen Knoll (Fig. 1). Like San Clemente Island's topography, the anticline forming the backbone of the island is also asymmetric with an axis lying about 1 km inland from the northeastern shore. Originally subhorizontal contacts between andesite flows now exhibit 10–30° dips on the northeastern flank and 0–10° dips on the southwestern side of the island (Smith 1897; Merifield *et al.* 1971). The steeper dips of the southwestern flank occur near the coast whereas the bedding is almost horizontal towards the crest of the island. As pointed out by Olmsted (1958), arching occurs not only perpendicular to but also parallel to the island's main axis, which plunges 2–3° toward its northwestern and southeastern ends. Olmsted was the first to describe San Clemente Island as an asymmetrical dome only slightly modified by secondary faulting. Nevertheless, the island is currently referred to as a tilted or uplifted crustal fragment driven by block faulting, and lying in a region characterized by Horst and Graben morphology inherited from Middle Miocene oblique rifting (Legg & Kennedy 1991).

2.5 The San Clemente Fault

The straight northeastern flank of San Clemente Island is bounded by a steep (15° average slope) N35°W-trending escarpment that extends 80 km from 15 km north of the island to south of Fortymile Bank (Figs 1, 3). Shepard & Emery (1941) first described this escarpment as a fault scarp, although they were puzzled by the fact that '...to the northwest this scarp hugs the island but when traced southeastward instead of dying out it is replaced by an escarpment which slopes in the opposite direction...'. They explained the similarity between the shape, size and rock types of San Clemente Island and Fortymile Bank as resulting from 40 km of right lateral slip along the fault itself. Olmsted (1958) tentatively mapped the San Clemente Fault as coincident with the escarpment but with a much steeper or even vertical dip. Olmsted entertained previous suggestions of this being a strike-slip fault, but pointed out that '...whatever the actual direction of movement may have been... the top of the island is more than a mile above sea floor northeast of the fault...'. Allen, Silver & Stehli (1960) proposed that the San Clemente Fault, southeast of Fortymile Bank, connects to the San Ysidro Fault and then with the Agua Blanca Fault, a major strike-slip fault that comes ashore in Baja California. Merifield *et al.* (1971) accepted the hypothesis that the San Clemente Fault is a major strike-slip feature, but they warned that its recognition was based primarily on physiography. Interpreting Seabeam and high-resolution reflection data, Legg *et al.* (1989) concluded that the San Clemente Fault is an active, northwest-trending, right-lateral, wrench fault. In Legg *et al.*s analysis, the significant relief observed along the fault relates to dip slip accompanying the creation of pull-apart basins at fault steps. Legg's (1991) summary model of California Continental Borderland evolution further stresses the possible roles of oroclinal buckling and oblique extension in the generation of large escarpments such as that bounding the northeastern flank of San Clemente Island.

Paradoxically, the San Clemente Fault can still be argued today as being: (1) a large normal fault, in part bounding a clockwise rotated block located between the island and the mainland; (2) a major right-lateral strike-slip fault, in analogy to the San Jacinto, Elsinore and nearby Palos Verdes faults; or (3) a reverse or thrust fault, in recognition of the anticlinal structure of the island. Although there is limited seismic activity near the San Clemente Fault, the earthquakes have mostly been too small to recover the focal mechanisms needed to substantiate any of these hypotheses. If anything, the variety of the few $M4$ and $M5$ focal mechanisms that have been recovered only serves to confuse the picture further. Legg & Kennedy (1991), for instance, report that the largest quake in the historical period ($M5.9$, 1951 December 26) occurred just off the southeastern edge of the island and had P-wave first motions consistent with *left-lateral* strike slip on a shallow surface trending nearly parallel to the San Clemente Fault.

Although the notion that the San Clemente Fault is pure right-lateral strike-slip along its entire length tends to be favoured in the literature, this idea is the most difficult of the three hypotheses to reconcile with geological data. Certainly some type of dip-slip must be invoked to explain San Clemente

Island's imposing height relative to the surrounding ocean floor. Near the island at least, there must be either footwall uplift caused by normal faulting, or hanging-wall uplift caused by reverse or thrust faulting. The 15° northeast-dipping slope of the San Clemente Island escarpment is much steeper than any other submarine feature in the region and might be the surface expression of a fault plane. Normal faulting on a northeast-dipping plane would raise San Clemente Island, but should have produced a trough of equal or greater extent in the Santa Catalina Basin. Such a depression does not appear in the bathymetry nor is it hidden by sedimentary cover (see the seismic reflection profile in Section 4.3). Normal displacement on a northeast-dipping, surface-breaking fault should have also produced a homoclinal, not anticlinal, setting of the island's deposits. Moreover, large-scale normal faulting is generally incompatible with the compressional style of present-day deformation in the California Continental Borderland as revealed by geodetic data (see Section 4.4). Thrusting on a northeast-dipping plane is not likely either, because San Clemente Island, being on the footwall, would be dropped and the sea-floor raised in that scenario. Although normal faulting on a northeast-dipping surface may have played a role in the tectonic development of the region in an earlier period, we believe that the only reasonable hypothesis is that the island's recent growth is driven by a southwest-dipping thrust or reverse fault.

2.6 Secondary faulting

Although none of the previous investigators described or hypothesized significant reverse or thrust faulting near San Clemente Island, many of them observed secondary strike-slip and normal faults. Most of these trend perpendicular to the island's long axis and modify only slightly its otherwise regular domal shape. Onshore, Olmsted (1958) described a swarm of N10°E-trending normal faults affecting the southern portion of the island (Fig. 4). North–south trending faults in this part of the Continental Borderland (e.g. Legg 1991) are regarded as witnessing a Neogene phase of regional east–west extension (Luyendik *et al.* 1985). The normal faults of southern San Clemente Island all share west-side-up displacement, yet Olmsted (1958) and Merifield *et al.* (1971) made no mention of vertical displacement of the younger terraces, and Muhs (1983) specifically remarked on the absence of detectable offsets. Offshore, Ridlon (1972) reported significant disruption of the 80–120 m deep encircling shelf by small but numerous northeast-trending normal faults. Feeling that the shelf was very young (Holocene or post-Wisconsin <20 ka), Ridlon concluded that these faults were extremely active. In Emery's (1958) opinion, however, the encircling shelf was cut by many lowerings of sea-level, and only part of it was planed during the Holocene lowstand. This explanation, with which we agree, drastically increases the age of the shelf and correspondingly reduces the slip rate of Ridlon's faults.

Although some of the youngest marine terraces have been influenced by secondary faults, most evidence points to their activity being surficial and very slow (slip rate <0.1 mm yr^{-1}). The existence of these secondary faults at best only causally relates to the much larger-scale and deep-seated thrust or reverse faulting that we hypothesize to have generated the island.

3 MODELLING APPROACH

3.1 Generalities—why terraces?

Our modelling approach assumes that San Clemente Island has grown from accumulated slip along surfaces embedded below it, and that by properly tracing the configuration of certain geological markers, characteristics of the driving faults can be inferred. Even the simplest application of geological geodesy using planar uniform slip faults (Stein, King & Rundle 1988; Valensise & Ward 1991; Ward & Valensise 1994; Hummon *et al.* 1994) has proved valuable in illuminating the shape and evolution of many fault-related geological structures and landscape features. Although a variety of geological markers (bedrock attitudes, sediment unconformities, sea-floor bathymetry) can be employed to track San Clemente Island's deformation, marine terraces, because they form at a specific elevation (sea-level) and time (highstands), offer the best clues. Moreover, unlike topographic elevations that can be affected by non-tectonic processes such as erosion and deposition, inner-edge elevations of marine terraces present a clean data set in the sense that the mere presence of the strandline means that the location has remained undisturbed after emergence.

Reconstruction of the San Clemente Island's terraces involves: (1) identifying numerous terrace and inner-edge fragments; (2) correlating them into complete strandlines; and (3) dating the strandlines if possible. Building on extensive material from past studies, we reconstructed the principal terraces from published inner-edge elevations, 1:24 000 scale topographic maps, the geological map supplied by Olmsted (1958), existing fossil ages and global sea-level curves (see the Appendix for details). Fig. 4 presents our terrace identification and correlation. (Potential terrace ages are elaborated later in Fig. 10.)

Given the uncertainties in the reconstruction, a prudent course in modelling first focuses on those aspects of fault geometry and tectonic style that can be deduced from the shape of the island platform independent of the age and mutual correlation of the terrace remnants. Once the geometry and style of the driving fault are established, a formation date for a reference terrace can be introduced to fix the average rate of uplift and therefore the rate of fault slip. In this way, most of the conclusions will be unaffected (fault style) or can be easily revised (slip rate) if new terrace correlations or absolute ages are proposed.

3.2 A base 2-D geological fault model

Noting the $\sim 20°$ bend in San Clemente Island's long axis (Fig. 4) and the differences between its southern and northern sections (A–A′ and B–B′, Fig. 2), it is likely that at least two fault segments are directing the island's growth. Given the fact that the simplest 3-D fault segment (uniform slip, rectangular patch) involves 10 parameters [strike, dip, rake, length, down-dip width, (x, y, z) position of an upper corner, slip, and a baseline level], we are confronted with an inverse problem with a minimum of 20 unknowns, far more than can be resolved simultaneously. A logical remedy first constrains certain of these parameters with a simplified 2-D geological fault model (2D-GFM) prior to 3-D modelling. We seek a 2D-GFM that reproduces individually the southern and northern profiles A–A′ and B–B′ (Fig. 2) by varying the five parameters [dip, down-dip width, (x, z) position of the upper corner, slip] of

2-D, purely dip-slip faults. Fig. 5 shows that even this five-parameter space encompasses a variety of uplift patterns. To reduce the unknowns further, the pre-deformation baseline level was fixed at 1000 m below today's sea surface, an elevation typical of the undisturbed ocean basins near San Clemente Island.

The heavy lines in the first and third panels of Fig. 6 trace 32 km long profiles B–B′ and A–A′. The profiles span the emerged island and stretch outwards across the submarine platform until they reach undisturbed ocean basin. These profiles provide evidence of the tip-of-the-iceberg role played by the visible island. Because the entire 20 to 30 km wide bulge was generated by faulting, a correct appreciation of the scale of the island-building mechanism can be obtained only by modelling the entire profile and not just the topmost emerged portion. The lighter lines in the first and third panels of Fig. 6 plot the uplift predicted from the best-fitting 2D-GFM depicted in the second and fourth panels. The first and third panels have vertical exaggerations of 5:1 to emphasize the quality of reproduction, while the second and fourth panels have virtually no exaggeration to show the induced anticline and the causative faults in their proper perspective. The observed and predicted profiles generally fit well. Mismatches, such as the submarine shelf at −120 m, probably result from unaccounted processes of erosion, deposition and secondary faulting.

The two observed profiles are fairly different in shape, with B–B′ being narrower and more symmetric than A–A′. Not surprisingly, the two fault segments that generate the uplift

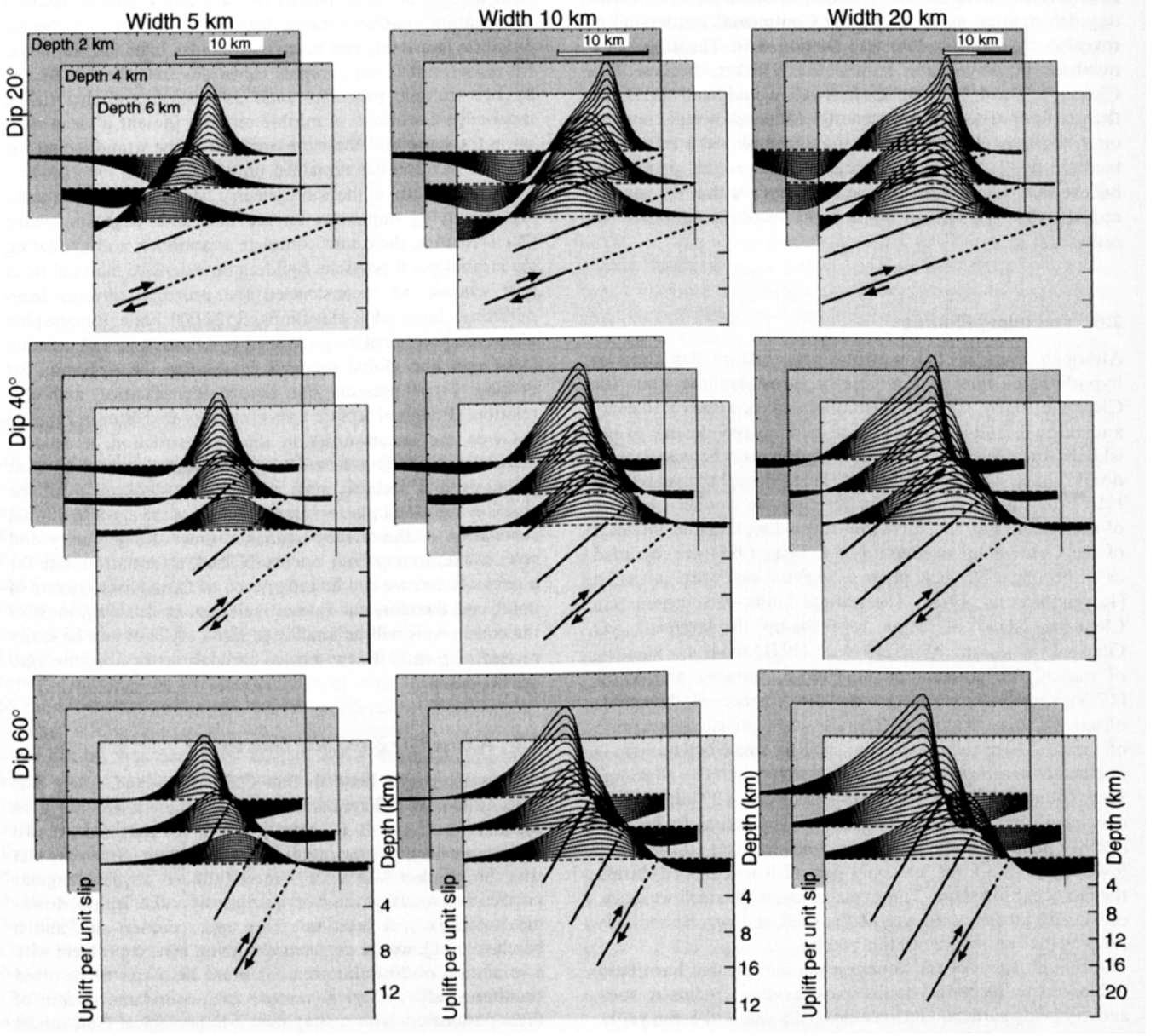

Figure 5. 2-D uplift patterns generated by progressive thrusting on a variety of buried inclined faults. The rows vary the fault dip from 20° to 60°. The columns vary the down-dip width of the fault from 5 to 20 km. The boxes show the effects of varying the depth to the top of the fault from 2 to 6 km. The underlying philosophy of our work is that many of the compressive structures in the California Continental Borderland are formed by accumulated fault action and that the different shapes of the structures are controlled by the different styles of the underlying faults.

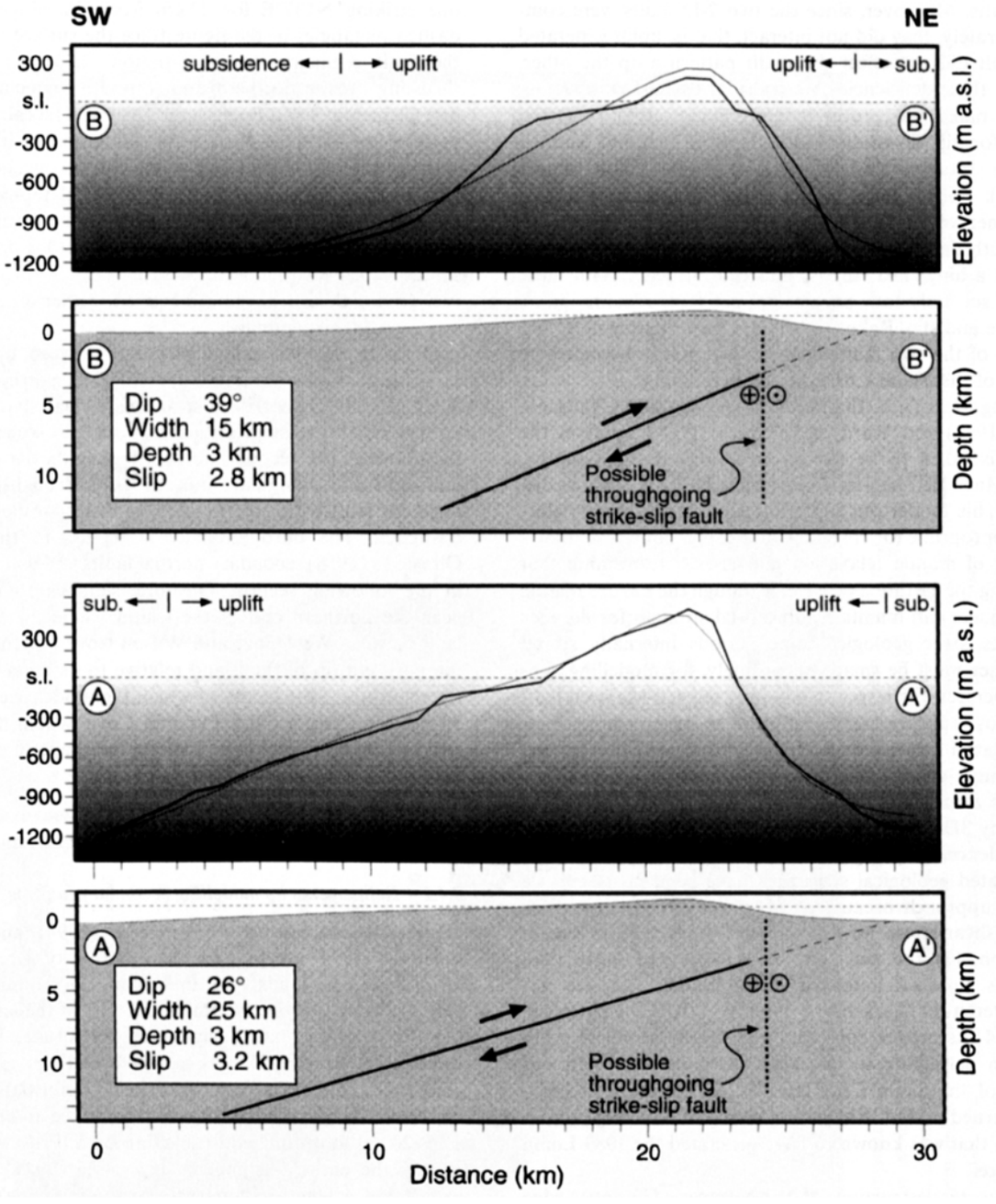

Figure 6. (Panels 1 and 3) Best-fitting uplift pattern (heavy lines) predicted from the 2D-GFM compared with observed San Clemente Island profiles (light lines) B–B′ and A–A′ of Fig. 2 at 5 : 1 vertical exaggeration. (Panels 2 and 4) Predicted uplift pattern and causative faults shown with no vertical exaggeration. The shape of San Clemente Island and its platform is best explained by blind thrusting on shallowly dipping planes. This explanation is inconsistent with a simple twist in a regional strike-slip fault, which was the case for the Palos Verdes Hills. Regional strike slip in this area may be partitioned onto a separate vertical through-going fault that surfaces near the trace of the thrusts.

have fairly different styles. To explain the narrower northern profile, the northern segment dips 39° and slips over a down-dip width of 15 km. To explain the wider southern profile, the southern segment must dip more shallowly (26°) and slip over a larger width (25 km). Both faults, however, fail to reach the surface, terminating at 3 km underneath the northeast edge of the island. Over timescales of millions of years, 2.8 and 3.2 km of slip on the northern and southern fault segments, respectively, have raised San Clemente Island from 1000 m below sea-level to 200 and 600 m above sea-level. Dramatic as this deformation may seem, however, the total strain in this mature system is only about 10 or 15 per cent (revisit the second and fourth panels of Fig. 6).

3.3 A base 3-D geological fault model

Although the 2D-GFM demonstrates that the shape of San Clemente Island and its platform are well explained by *blind thrusting on shallowly dipping planes*, it cannot constrain the ratio of strike slip versus dip slip or the lateral extent of the

driving faults. Moreover, since the two 2-D faults were computed separately, they did not interact; that is, uplift generated by one fault did not affect the uplift pattern atop the other. To remedy these deficiencies, we consider two 3-D interacting faults. To make the process manageable, values from the 2D-GFM for dip, down-dip width, depth to top, and baseline level were retained in the 3-D geological fault model (3D-GFM). Furthermore, the (x, y) location of the southern upper corner of the northern fault segment was made to coincide with the northern upper corner of the southern fault segment at a hinge near the island's central bend. With these conditions set, only four parameters per fault remain: strike, length, rake and slip. Rake and slip are linear parameters, and the strikes of the two fault segments are tightly bounded by the trends of the island's straight northeast faces.

Following Matsu'ura, Tanimoto & Iwasaki (1981), Valensise & Ward (1991) and Ward & Valensise (1994), uplift in the 3D-GFM is taken to be the response of a non-gravitating, viscous (Maxwell) half-space to uniform slip planar dislocations. This model can reproduce elastic half-space deformations appropriate for coseismic modelling, but it also allows for aspects of mantle relaxation and crustal restraining that occur during the earthquake cycle. Although the Earth's mantle and lithosphere can maintain substantial strength for decades or centuries, over geological time periods internally stored shear stresses must be small. Accordingly, for modelling geological structures, the response of a fully relaxed Maxwell half-space is most appropriate. In addition to its vanishing shear stress, a relaxed half-space has the useful property that the net surface-volume change due to *any* distribution of shear dislocations is zero (Ward 1986). Thus, the long-term actions of faults in any 3D-GFM always induce equal volumes of uplift and subsidence. Although several methods for modelling fault-generated geological structures have been proposed, we justify this approach because of: (1) its nice theoretical traits (vanishing shear stress, no net volume change); (2) its ease of computation; (3) the fact that its smooth and fairly mild adjustments produce long-term deformations that are not terribly different in character or dimension from the coseismic field; and (4) its proven consistency in situations where other information pertaining to the causative faults exists. In our modelling of the Santa Cruz terraces, for instance, the procedure returned a 3D-GFM with a configuration very similar to the fault that was known to have generated the 1989 Loma Prieta quake.

From our reconstruction of the terraces, 432 inner-edge locations and heights were sampled at an average spacing of 300 m along terraces 2 to 13 and the '1500 ft terrace'. These data and 128 elevations along four topographic transects (two across-width profiles, A–A′, B–B′; plus two length-parallel profiles, one through the island's centre and one about 20 km to the west) were inverted for strike, length, rake and slip. After a few test inversions it became clear that, unlike the Palos Verdes Hills, San Clemente Island lacks significant along-strike asymmetry, and, by implication, strike-slip displacement on the underlying thrusts must be small. Although strike slip might be occurring on nearby structures, our models were constrained to pure thrust faults.

Fig. 7 compares the observed topography (left) with topography generated by the best-fitting 3D-GFM (right) that consists (largely) of two misaligned blind thrusts—a northern one striking N27°W for 15 km from the hinge and a southern one striking N137°E for 22 km from the hinge. The white dashed rectangles in the figure trace the surface projection of the fault segments. Since initiation, 2.55 and 3.43 km of thrusting on the northern and southern segments raised the San Clemente Island dome some 1600 m. The calculated uplift pattern fits the long-wavelength topography fairly well considering the simplicity of the uniform-slip rectangular faults which make up the 3D-GFM. The model reproduces nicely the progressive coalescence of the two proto-islands, outlined by the bottleneck shape of Terrace 8 (see Fig. 8, right). The simultaneous emergence of the proto-islands suggests that the two driving thrusts have been active together for a substantial fraction of their lifetime.

Offshore, smaller-scale departures between observed and model topography are found at Eel Point, Northwest Harbor, and Pyramid Cove. The first anomaly relates to a deep but narrow north-trending canyon that was cut sometime during the doming. The second anomaly highlights the simplicity of uniform-slip rectangular fault models. Probably, a longer, northern fault with tapering slip or width would explain the mismatch. The third anomaly is related to the action of Olmsted's (1958) secondary normal faults and will be discussed in the following section. Onshore, significant misfits occur: near the northern end of the island where an east-trending fault between West Cove and Wilson Cove evidently displaces the northern tip of the island relative to its main body; along the main ridge, the length of which the model overpredicts by 30 per cent; and around Pyramid Cove, where the action of shallow normal faults mildly affects the shape of the youngest and lowest portions of island.

3.4 Refinements to the 3-D geological fault model

3.4.1 Refinements by modelling secondary faulting

Significant conclusions of Valensise (1994) and Ward & Valensise (1994) are that the deformation of a region's landforms is a consequence of the combined straining from all tectonic sources active within the lifetime of the landform, and that each source has a signature magnitude, pattern and wavelength. Sensibly, large-scale deformations require large-scale tectonic sources, and short-scale deformations require small-scale sources. For instance, to produce an anticline with a 15–20 km footprint requires action on a thrust with a width cutting the entire seismogenic layer (see Fig. 5, upper right panel) and a length comparable to the anticline's along-axis extent. Likewise, motion on a shallow fault cutting just to bedrock will only disturb a region over a width comparable to the depth to the basement. Supposing that maximum cumulative slip on a mature fault amounts to some fraction of its width (say, 10 per cent) and that the vertical deformation produced amounts to some fraction of the cumulative slip (say, 30 per cent), then the magnitude of potential deformation also scales with source size. 1 km of uplift might require a 30 km [$\sim 1\ \text{km}/(0.1 \times 0.3)$] fault, while a 100 m high landform might be generated by a 3 km fault.

This reasoning can be used to untangle signals from tectonic sources of different scales. For instance, mismatches between the structure generated by the base 3D-GFM and the actual shape of the island were mostly an order of magnitude smaller than the size of the two main driving fault segments. The only means to improve the fit is to include additional smaller-scale

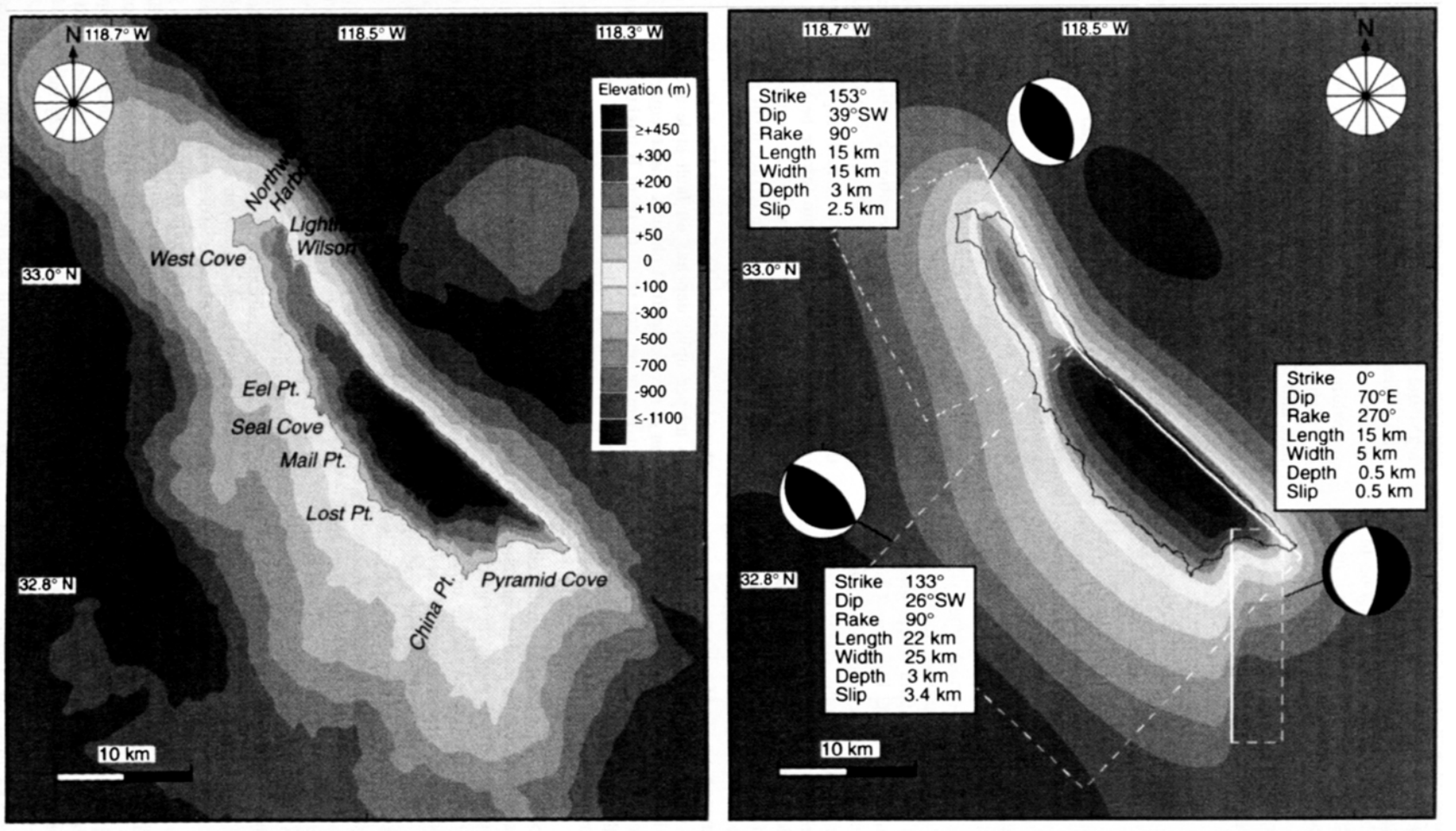

Figure 7. (Left) Expanded view of the topography/bathymetry of the San Clemente Island region. Note that the offshore bathymetry mimics the shape of the island. The emerged land is just the tip of a much bigger structure, most of which is below sea-level. The entire structure is presumed to be fault-generated, but there is no on-land evidence for such a fault. (Right) Topography/bathymetry generated by the best-fitting 3D-GFM, which consists of two misaligned blind thrust segments whose surface projections are indicated by the white dashed rectangles. Since initiation, 2.5 and 3.4 km of thrusting has occurred on the northern and southern faults, raising the dome from 1000 m below sea-level to 600 m above sea-level. By and large, the genesis of San Clemente Island is well explained by progressive slip on the two major thrust segments; however, secondary faults with perhaps 500 m of slip have distorted the topography on a smaller scale. As illustrated here, the bite missing from the island's southeast end (see also Fig. 4) can be attributed to the action of a set of north–south-striking normal faults.

sources of deformation, that is, one or more secondary faults. Following Olmsted's (1958) indication that the western side of Pyramid Cove is bounded by a significant N10°E, west-side up normal fault (Fig. 4), we searched for a secondary fault to minimize the discrepancies between predicted and observed topography near the southern tip of the island. A good fit is obtained for a north-trending, subvertical, normal fault nearly coincident with one mapped by Olmsted (Fig. 7). Compared to the main driving faults, cumulative slip (0.5 km) and down-dip width (5 km) are small (~20 per cent) on this secondary fault, yet it has carved a very visible wedge out of the island's southern end.

3.4.2 Refinements from drainage patterns

Owing to its remote location, its relative youth, and its limited erosion rate, San Clemente Island is a good laboratory for exploring relationships between tectonics and drainage networks. Characterization of drainages largely reduces to the depth and direction of their channels. While incision depth is a complex function of local bedrock lithology, stream gradient, and water supply, stream direction is almost time-, climate- and lithology-independent. Driven by gravity, streams prefer to go downhill, following the steepest path where given the choice. In regions of continuing uplift, like San Clemente Island, bits of new land exposed at the coast are subject to incision by streams following the topographic gradient oriented perpendicular to the shoreline that existed at the time. Once cut, the new stream sections become 'locked' in place and are generally impervious to subsequent changes in the local direction of topographic gradient. Thus the evolving hierarchy of drainage becomes a permanent record of palaeotopographic gradient directions and a window on evolution history. For example, normal Fault A in Fig. 8 was active at the time of carving of Terrace 12 and controlled the direction of stream S. The fault then switched off prior to the carving of Terrace 9, leaving the S-shaped stream as an artefact of its short period of activity.

The effects of time-dependent processes are reflected in differences between the present topographic gradient directions and the directions of drainages. Fig. 9 plots the gradients calculated from the 3D-GFM superimposed on the drainage network in the southern half of San Clemente Island. In several places, stream directions differ from the current gradient directions—along the 'S' stream, and around Pyramid Cove where drainage is focused towards the centre of the bay through the action of a secondary normal fault. Interpretation of palaeotopographic directions by means of drainage patterns is a new area of research that we are trying to quantify as a means to improve evolutionary models like Fig. 8.

4 DISCUSSION

4.1 Timing of uplift—implications for fault slip rates

Section 3 sketched a clear picture of the geometry and style of faulting under San Clemente Island. To finish the artwork, rates of deformation and dates of initiation need to be brushed in. Recall from Section 2, that direct, but incomplete, fossil ages of 127 ± 7 and 111 ± 3 ka exist for Terrace 2. Based on the Lajoie *et al.* (1991) sea-level curve, the first of these ages corresponds to 124 ka stage 5e, which had a highstand elevation 6 m above today's sea-level. The second age falls between highstands 5e and the 102 ka stage 5c, which had a highstand elevation 7 m below today's sea-level. To help resolve ambiguities in direct dating, additional, but indirect, height information from all the terraces can be included in a common procedure (Lajoie 1986) that correlates the inner-edge elevations of a flight of terraces with the expected heights given highstand ages and formation elevations from a global sea-level curve. Fig. 10 shows how the procedure works. The jagged curve along the bottom-left traces the height of the global oceans versus age. The uneven steps to the right give the heights of the terrace surfaces. The slanted broken lines project the potential elevation of terraces that may have been cut at each highstand assuming a constant, but unknown rate of uplift. By searching a range of uplift rates and by judging the degree to which observed terraces fall at predicted elevations, uplift rates and sets of terrace ages can be proposed. The exercise reveals good correlations with the sea-level curve for uplift rates of 0.2, 0.33 or 0.45 mm yr^{-1}. As a consequence, ages of 81, 102 or 124 ka for Terrace 2 are equally plausible (see the Appendix).

With the style of the 3D-GFM established in Section 3, the amount of fault slip that has occurred since the formation of a terrace can be determined from the net terrace uplift (current elevation minus terrace formation elevation), as outlined in Ward and Valensise (1994). Dividing 'slip since formation' by the age of the terrace returns a fault slip rate. Terrace uplift rates could be extracted from terrace heights and a sea-level curve alone (as done in Fig. 10); however, a geological fault model is needed to translate terrace uplift rates into fault slip rates because there is not a universal correspondence between these two quantities. As shown in Fig. 5, the ratio of fault slip to terrace uplift depends on fault style and varies spatially. 1 m of terrace uplift at point **A** might require 4 m of fault slip, but 1 m of terrace uplift at point **B** might require just 2 m of fault slip. Likewise, 1 m of terrace uplift at a fixed point **C**, might require 3 m of slip for a fault dipping 30° but 4 m of slip for a fault dipping 20°.

Three options exist for the age and net uplift of Terrace 2: 124 ka, 26 m (32 m current elevation minus 6 m formation elevation); 102 ka, 39 m (32 m current elevation minus −7 m formation elevation); and 81 ka, 44 m (32 m current elevation minus −12 m formation elevation). Given our 3D-GFM and the location of Terrace 2, 63.1 m of slip on the northern fault and 82.7 m of slip on the southern fault would best reproduce the 26 m of net uplift needed if Terrace 2 was cut during the 124 ka highstand. Fault slip rates for this case would be 0.51 and 0.67 mm yr^{-1} respectively. Fig. 11 plots these values as triangles and circles on the vertical slip-rate bar labelled 124 ka. Fig. 11 also summarizes comparable calculations for the possible 102 and 81 ka ages of Terrace 2. Younger age assignments translate into faster rates of fault slip. Average rates for the northern and southern faults are 0.51, 0.92, 1.32 mm yr^{-1} and 0.67, 122, 1.73 mm yr^{-1}, respectively, for a 124 ka, 102 ka and 81 ka Terrace 2. Assuming these rates were constant over time, the inception ages of the faults are just their total slip divided by their slip rate. The northern and southern fault ages of inception are: 2.55 km/ [0.51, 0.92, 1.32] mm yr^{-1} = 5.0, 2.8, 1.9 Ma; and 3.43 km/ [0.67, 122, 1.73] mm yr^{-1} = 5.1, 2.8, 2.0 Ma. Although it was not a constraint, the agreement in ages between the two faults suggests that they initiated simul-

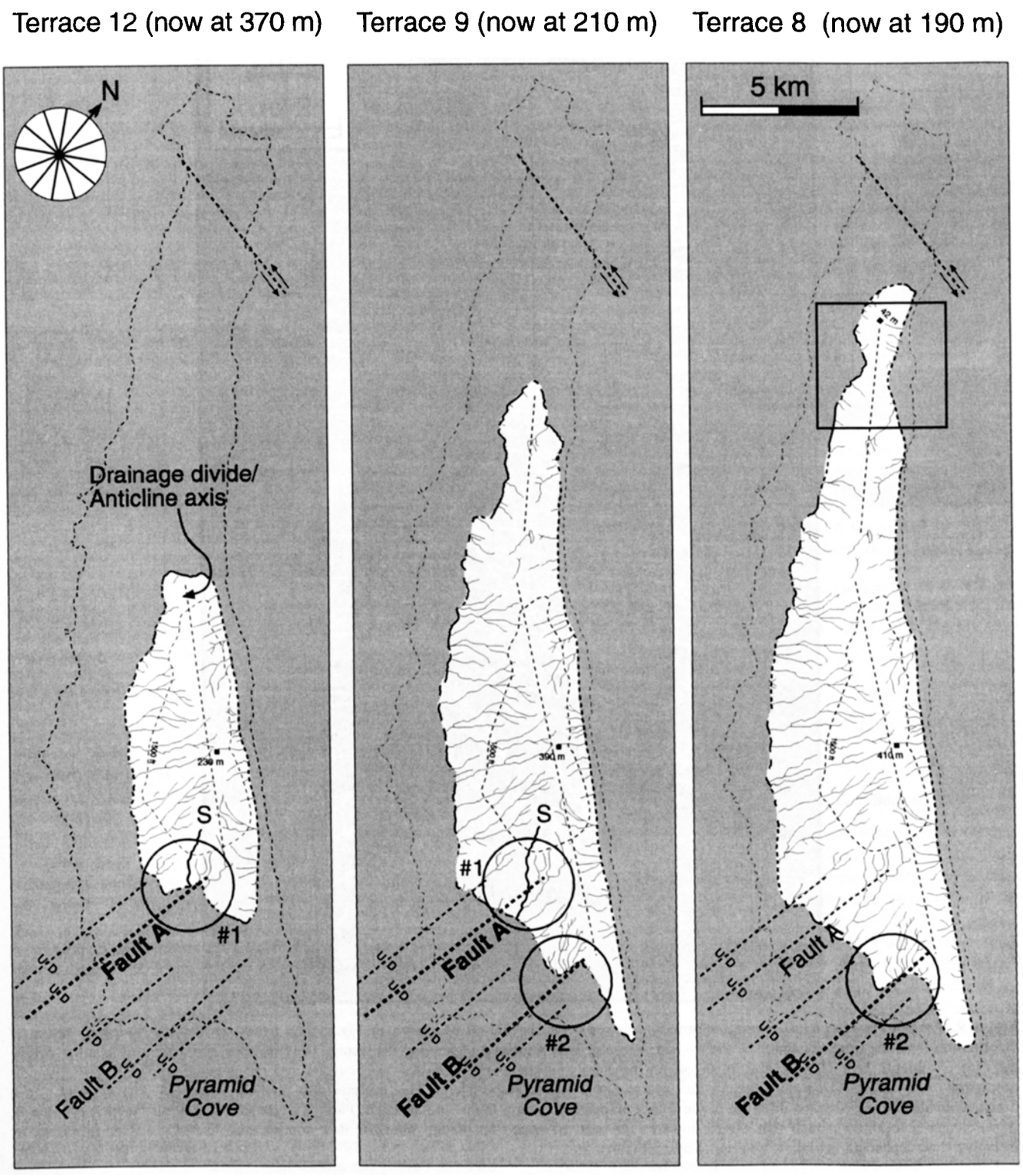

Figure 8. Reconstruction of shorelines and drainage patterns associated with terraces 12, 9 and 8. Each reconstructed shoreline is nearly a scaled version of the adjacent ones, and the essential features of the island, such as the longitudinal symmetry of the island with respect to its highest peak, the asymmetric location of the drainage divide, the straightness of its eastern flank, and the convex shape of its western flank, persist for time-scales of over 1 Myr (presumable the age of Terrace 12). Notice the bottleneck shape of Terrace 8 (shown by a box), where its shoreline encircles a localized high on the northern half of the island. This condition may reflect the coalescence of two separate centres of uplift, each driven by a separate fault segment (see also the trend of the 100+ m contour in Fig. 7, right). Also notice the role played by secondary faulting in distorting the shorelines and diverting the drainage.

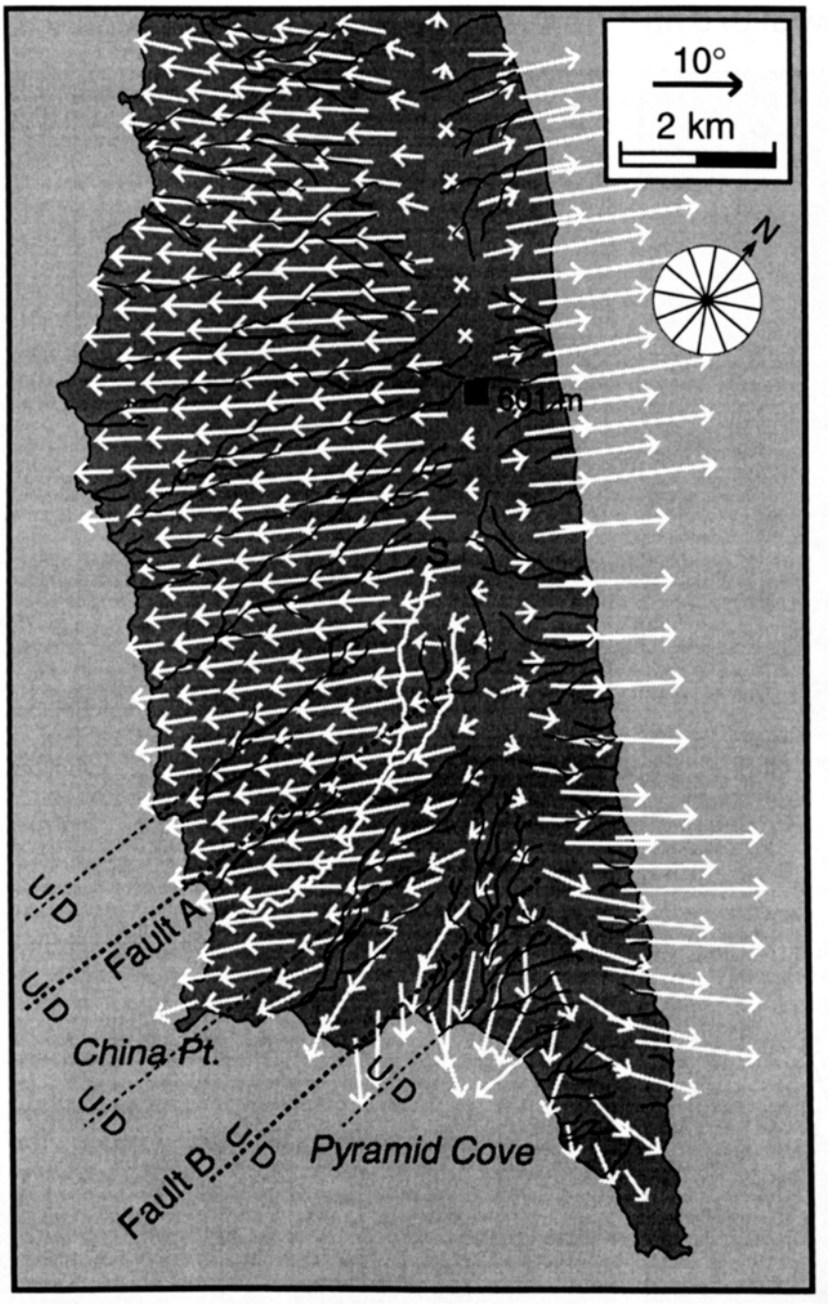

Figure 9. Predicted gradients of vertical deformation (arrows) for the 3D-GFM shown in Fig. 7. The figure stresses the anticlinal nature of deformation resulting from the action of the two large reverse fault segments underlying the island. The predicted gradients match rather closely the dips of andesite beds (10–30° and 0–10° on northeastern and southwestern flanks, respectively) and the average gradients of the island's topography (22° and 5–8° on northeastern and southwestern flanks, respectively). This exercise also predicts successfully the position of the drainage divide and the effect on drainage of previously mapped secondary faults. In particular, Fault B (same as in Fig. 8; also modelled in Fig. 7, right) creates a localized trough that diverts towards the east drainage that would otherwise flow southwards. The fit could be improved by including time-dependent actions of additional normal faults.

taneously. Of the three ages, we favour the 5.0 Ma value associated with the 124 ka highstand in deference to the direct fossil ages and the pronounced expression of the 124 ka terrace elsewhere in California. Over 5 Ma, 0.6 mm yr^{-1} of slip on the thrusts would have raised the island's centre of uplift (600 m elevation) some 1600 m at a pace of (1600 m/5 Ma) 0.32 mm yr^{-1}. First emergence would have occurred in the lower Pleistocene, around (600 m/0.32 mm yr^{-1}) 1.9 Ma.

4.2 Model predictions versus bedrock geology

The 3D-GFM makes several predictions that, to some degree, can be tested against independent geological observations.

(1) *Retrodeformation of the San Clemente Island anticline and removal of young continental and terrace deposits restores a nearly level sea-floor with depths in excess of 1000 m.* Initial

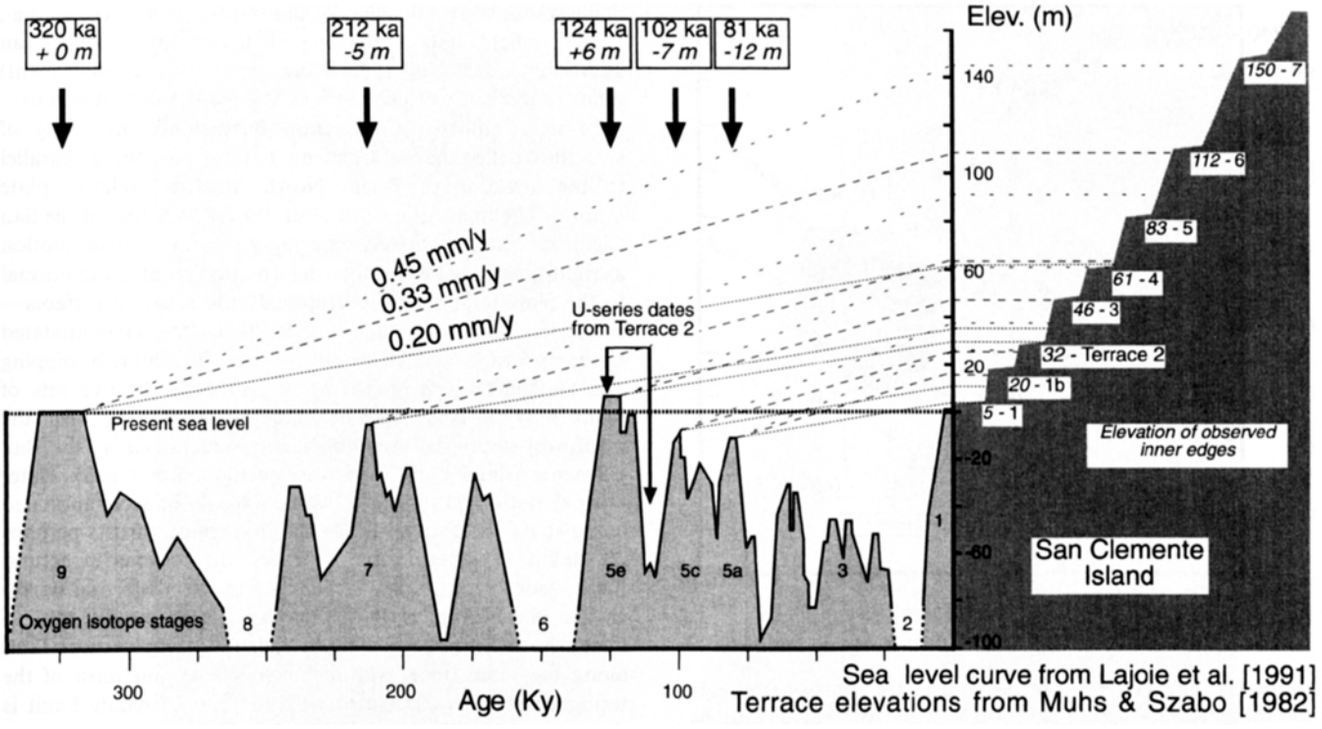

Figure 10. Correlations of the San Clemente terrace sequence (staircase on right) with the global sea-level history (jagged curve at bottom). Measured fossil ages of 111 ± 3 and 127 ± 7 ka for Terrace 2 are indicated, as are the age and formation elevation of the major highstands. The slanted broken lines project the elevation of terraces that could have been cut at each highstand assuming a constant rate of uplift. Equally good correlations with the sea-level curve give possible ages of 81, 102 or 124 ka for Terrace 2.

conditions of this type are unspectacular. Flat-lying Middle Miocene andesites overlain by Upper Miocene to Lower Pliocene deep ocean sediments are observed today over large undeformed sections of the California Continental Borderland (Moore 1969).

(2) *Deformation, proceeding at constant speed, was accomplished in 2–5 Myr.* A minimum age for the inception of faulting is constrained by the contrast between the Middle Miocene to Lower Pliocene marine sediments (4–15 Ma) and the overlying Upper Pliocene to Lower Pleistocene section (1–3 Ma). The Miocene sediments formed on a deep ocean floor whereas the Pliocene to Pleistocene section accumulated in a more coastal environment. The shallower-water faunas and the intercalated conglomerates forming most of this section (Stadum & Susuki 1976) may record the first passage of the inflating dome through wave-base, perhaps 100 m below modern sea-level. At that time San Clemente Island formed a sea-floor high analogous to the modern banks of the Continental Borderland with a total relief of 900 m. Uniformly proceeding deformation at our preferred rate fixes first emergence at 1.9 Ma or earlier, well within the period covered by the correlative Fernando Formation of coastal southern California.

(3) *Progressive growth produced a distinctive anticlinal setting for the lava flows and overlying marine deposits.* The distinctive dips of the predicted doubly plunging anticline are matched rather well by surface topography and bedrock geology. The increasing continuity and progressive thickening of the marine sedimentary apron from zero along the anticline axis, to 100 m in downthrown fault blocks or small synclines further off axis, to 200 m offshore, are also symptoms of progressive anticlinal folding.

4.3 Model predictions versus seismic reflection data

Potentially, seismic reflection data could validate or invalidate predictions of the 3D-GFM. Seismically imaging the main blind thrusts, however, may not be simple considering the facts that: (1) compared to other Miocene age structures in the region, the thrusts are relatively young (2–5 Ma) and possess modest amounts of deformation (2–3 km) and stratigraphic relief; and (2) the thrusts are fairly deep. Under the island, they reach to within 3 km of the sea-floor, but offshore to the west of the island, where they could be detected by seaborne reflection surveys, the faults lie between 6 and 14 km depth (1000 m reference).

The most relevant seismic reflection data that we are aware of is Line no. 120 of Bohannon & Geist (1966), which runs N56°E, southwest to northeast and approaches to within 4 km of the southern edge of San Clemente Island. Fig. 12 overlays a portion Bohannon & Geist's (1966) interpreted cross-section of Line no. 120 (bottom) on our proposed faults. It can be seen that Line no. 120 barely cuts the southern down-dip edge of the larger thrust, but that it slices the shallow eastward-dipping normal fault at its middle. The intersections of Line no. 120 and these two faults are indicated in the cross-section, as are their senses of motion. The major thrust intersects below the 6.6 km (1000 m reference) maximum depth of the survey in a seismically featureless body of Catalina Schist of Cretaceous to Jurassic Age. On the other hand, the proposed

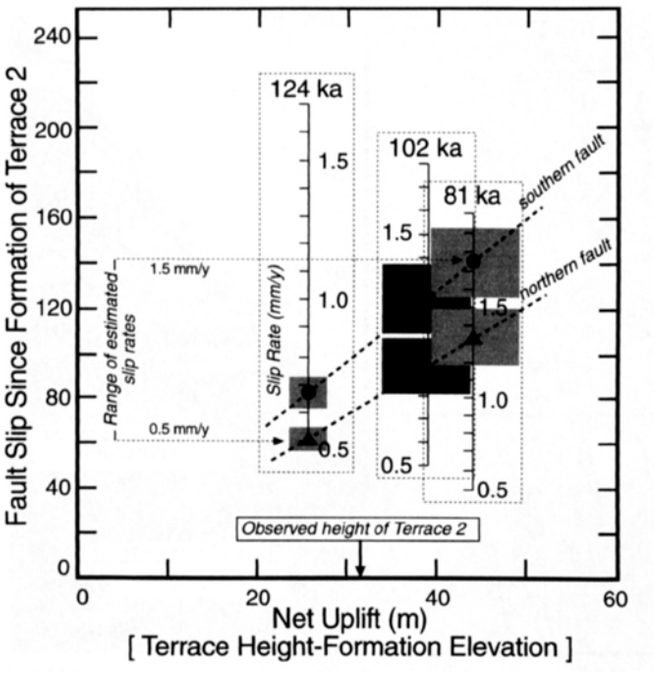

Figure 11. With knowledge of the style of the two fault segments underneath San Clemente Island, slip since terrace formation can be determined from net terrace uplift. For Terrace 2, three possibilities exist for terrace age and net uplift: 124 ka, 26 m; 102 ka, 39 m; and 81 ka, 44 m. The circles and triangles give the slip rates for the southern and northern fault segments for these three possibilities. The grey regions span the uncertainty in rates resulting from uncertainty in formation elevation (assumed to be ± 2 m for the 124 ka highstand and ± 5 m for the 102 and 81 ka highstands). Average rates for the two segments fall between 0.6 and 1.5 mm yr^{-1}.

normal fault (white in the figure) intersects at almost the exact location where the survey images a distinct eastward-dipping, listric-looking normal fault that extends from the sea-floor to about 5 km depth. Immediately eastwards from the island, the survey reveals a small pond of Pliocene and Quaternary sediments less than 4 km wide and 1 km thick, followed by a 7 km stretch of outcropping Catalina Schist.

Although existing seismic data are unable to argue for or against the existence of the proposed thrusts, we find it encouraging that the data do confirm the existence of a smaller normal fault whose presence was predicted solely from the deformation pattern of the island and its terraces. Moreover, the lack of a deep sediment-filled basin towards the east further counts against the idea that Pliocene uplift of San Clemente Island resulted from footwall uplift on an east-dipping normal fault.

4.4 Implications for slip partitioning

The clearest conclusion from our modelling is that the shape of San Clemente Island and its platform are well explained by *pure thrusting on shallowly dipping, blind fault segments*. As we know, blind compressional faulting also uplifted the Palos Verdes Hills; however, the similarities in fault style between the Palos Verdes and the San Clemente faults are not strong. The Palos Verdes Hills were induced by a simple steeply dipping ($\sim 65°$) restraining-bend twist in a through-going, right-lateral strike-slip fault. Both the shallow dip of the faults deduced above and the fact of their releasing-, not restraining-, bend configuration (supposing that they may possess an additional unresolved right-lateral component of movement) point to distinct tectonic mechanisms for the two situations.

In the California Continental Borderland, the string of structures called the San Clemente Fault strike roughly parallel to the direction of Pacific–North American relative plate motion. The implication from our 3D-GFM is that, if the San Clemente Fault is actively carrying a portion of plate motion as right-lateral strike slip, then deformation parallel and normal to the plate boundary is partitioned onto separate surfaces—somewhat like how oblique subduction is often accommodated by compression and strike slip on sets of shallowly dipping and vertical faults respectively. In our case, the two sets of faults may lie close together, emerging under or near the northwest–southeast trending features identified as the San Clemente Island Fault (geometry cartooned in Fig. 6). Plate-normal motion on such a fault system would be accommodated along-strike on discontinuous 'flap-like' blind thrusts perhaps 20–40 km in length dipping under the various structural highs—southwest in places such as San Clemente, and northeast in places such as Fortymile bank. Plate-parallel motion might be accommodated on a through-going vertical fault along the same trace. Although we believe that most of the topographic relief associated with the San Clemente Fault is thrust-generated (for example the Escarpment), the relief could also conceal the trace of a through-going vertical strike-slip fault whose motion has not left a strong imprint on the topography.

Potentially, GPS could help evaluate the extent of slip partitioning on the San Clemente Fault. Unfortunately, existing GPS data are sparse and subject to interpretation. Fig. 13 shows two estimates of GPS-determined tectonic velocities in the southern California Continental Borderland with respect to Catalina Island (BRSH). The top-row velocities were computed by Feigl *et al.* (1993) and the bottom-row velocities are from Larson (1993). At the left and right sides are the velocity components normal and parallel to the San Clemente Fault. GPS data in this region are fuzzy at the level of 3–4 mm yr^{-1}, but they allow 1 to 4 mm yr^{-1} of fault-normal compression across the Borderland. This is certainly compatible with our proposal that the San Clemente Fault is absorbing 0.6–1.5 mm yr^{-1} of thrusting near San Clemente Island. For strike slip, GPS supports 4 to 7 mm yr^{-1} across the Borderland. Localizing the displacement to individual faults is not possible, but with the Palos Verdes Fault taking some 3 mm yr^{-1} from the budget (Ward & Valensise 1994; McNeilan *et al.* 1996), perhaps 1–4 mm yr^{-1} might be partitioned on a vertical San Clemente Fault as proposed above.

4.5 Implications for seismic hazard in the Borderland

Although Feigl *et al.*s GPS data place more compression normal to the San Clemente Fault, Larson's data indicate more strike slip. Because both rates contribute to the strain and seismic hazard, the two models are actually fairly consistent in magnitude, with area-averaged strain rates of $\dot{\varepsilon} = 4.8$ and 2.5×10^8 yr^{-1} respectively. When translated using Kostrov's formula (Ward 1994) into an annual seismic moment-release rate $M \approx 2\mu AH\dot{\varepsilon}$, the strains supply 2.5 to 4.9×10^{17} N m yr^{-1} (for $H = 10.4$ km, $\mu = 3 \times 10^{10}$ Pa, and $A = 16\,363$ km^2) of earthquake potential offshore from San

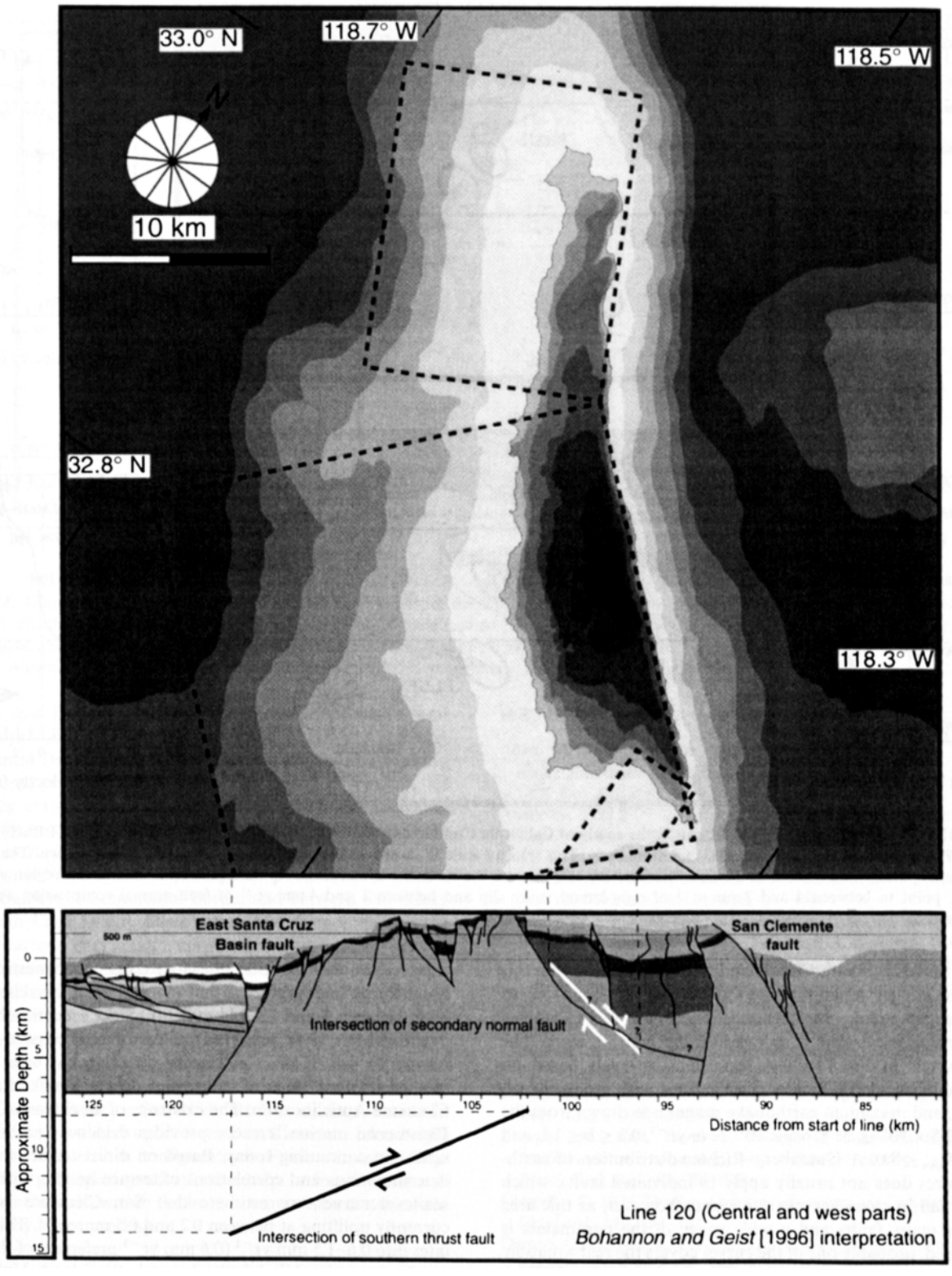

Figure 12. Bohannon & Geist's (1996) interpreted depth section of seismic reflection Line no. 120 (bottom) overlain on a topographic map of the San Clemente Island region. The surface projection of the three faults of the 3D-GFM are indicated as dashed lines. Line no. 120 cuts across the two southern faults, and the intersections are indicated in the depth section. The main thrust (black) is too deep to be imaged; however, the predicted east-dipping normal fault (white) is well expressed, as is the general domal shape of the island platform. Note the numerous small (2–3 km) normal faults that are riding the surface of the growing anticlinorium.

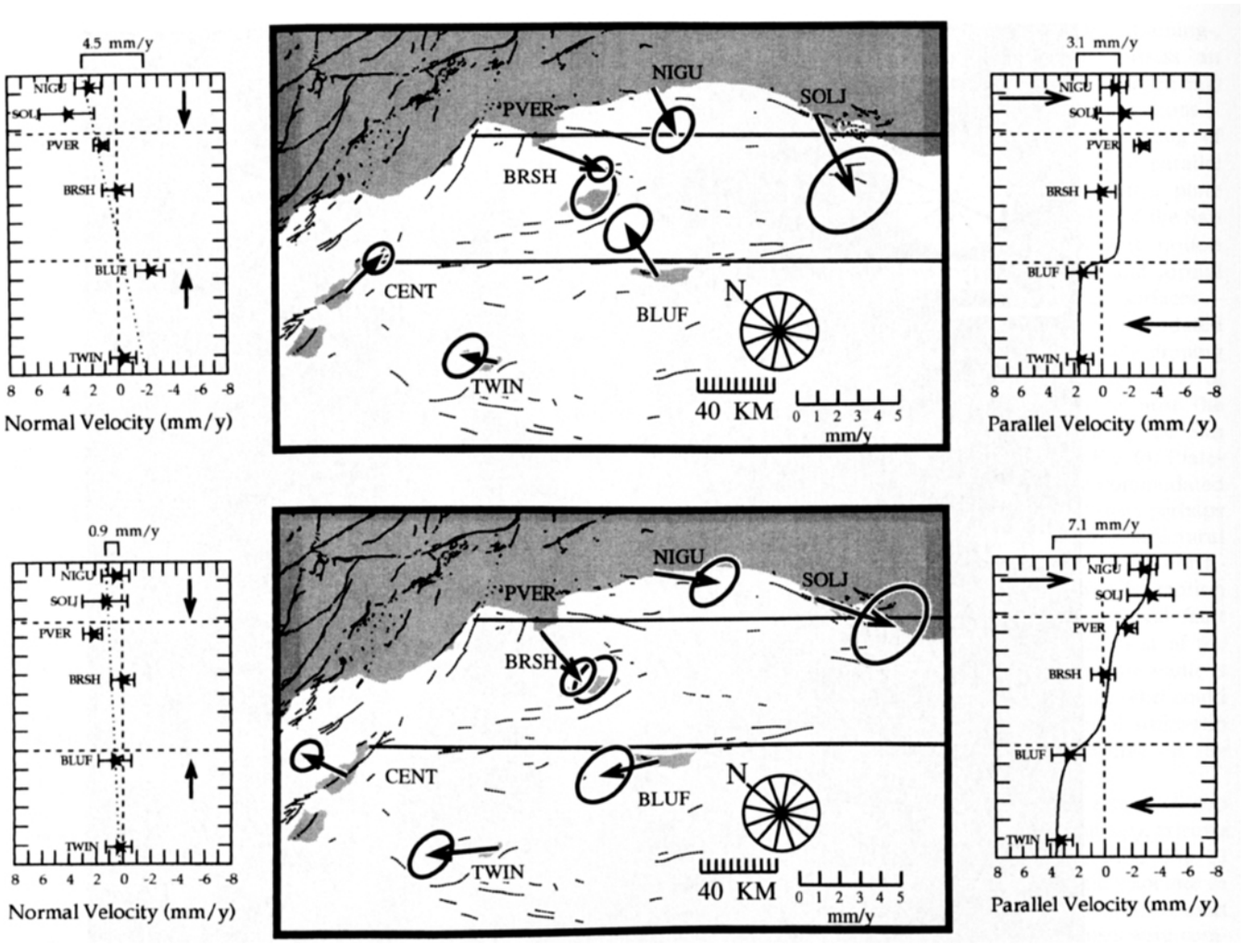

Figure 13. GPS estimates of tectonic motion in the southern California Continental Borderland with respect to Catalina Island (BRSH) by Feigl *et al.* (1993) (Top row) and Larson (1993) (Bottom row). The velocity scale is shown to the right and 3σ error ellipses are shown. The velocity components parallel and normal to the San Clemente Island Fault are shown to the left and right in each row. GPS data in this region are fuzzy, but they point to between 4 and 7 mm yr^{-1} of right-lateral strike slip and between 1 and 4 mm yr^{-1} of fault-normal compression across the Borderland.

Diego (SOLJ) to Santa Cruz Island (CENT). Distributing this moment budget among various earthquake magnitudes to estimate earthquake recurrence intervals for the California Continental Borderland is speculative, but worth a word. The three panels of Fig. 14 show recurrence intervals based on truncated Gutenberg–Richter distributions with moment rate, *b*-value, and maximum earthquake magnitude drawn from the ranges $2.5 \times 10^{17} \leq M \leq 6.5 \times 10^{17}$ N m yr^{-1}, $0.3 \leq b \leq 1.1$, and $7.2 \leq M_{max} \leq 8.0$. A Gutenberg–Richter distribution of earthquake sizes does not usually apply to individual faults, which tend to fail in characteristic size events; however, as this area encloses many faults and a wide range of the parameters is considered, probably one of the curves covers the real situation. This exercise suggests that, for this piece of the Borderland, *M*6+ earthquakes could recur at 27–77 yr intervals, whereas *M*7+ quakes might be encountered at 307–576 yr periods.

5 CONCLUSIONS

We find that the genesis of San Clemente Island and its surrounding submarine platform is consistent with progressive slip on at least two, southeast-striking, southwest-dipping, blind thrust fault segments that involve all of the seismogenic layer between 3 and 12–14 km depth. Since inception between 2 and 5 Ma (5 Ma preferred), 3 km of compressive motion normal to the N150°E fault strike direction has been accommodated with 1700 m of concurrent dormal uplift of the San Clemente Anticlinorium. The existence of an extensive suite of Pleistocene marine terraces provides evidence that slip and uplift are continuing today. Based on direct terrace fossil age determinations and correlations of terrace heights with global sea-level curves, we estimate that San Clemente Island is currently uplifting at between 0.2 and 0.5 mm yr^{-1}. This translates into 0.6–1.5 mm yr^{-1} (0.6 mm yr^{-1} preferred) of thrusting on the causative blind faults beneath the island. Unlike the situation beneath the Palos Verdes Hills, where a simple twist in a regional strike-slip fault accommodates both fault-parallel and fault-normal motions, the shallow dip of the thrusts suggests that, if regional strike-slip motion on the San Clemente Fault exists, it must be partitioned onto through-going surfaces distinct from the thrusts.

Existing GPS data are sparse and equivocal, but they

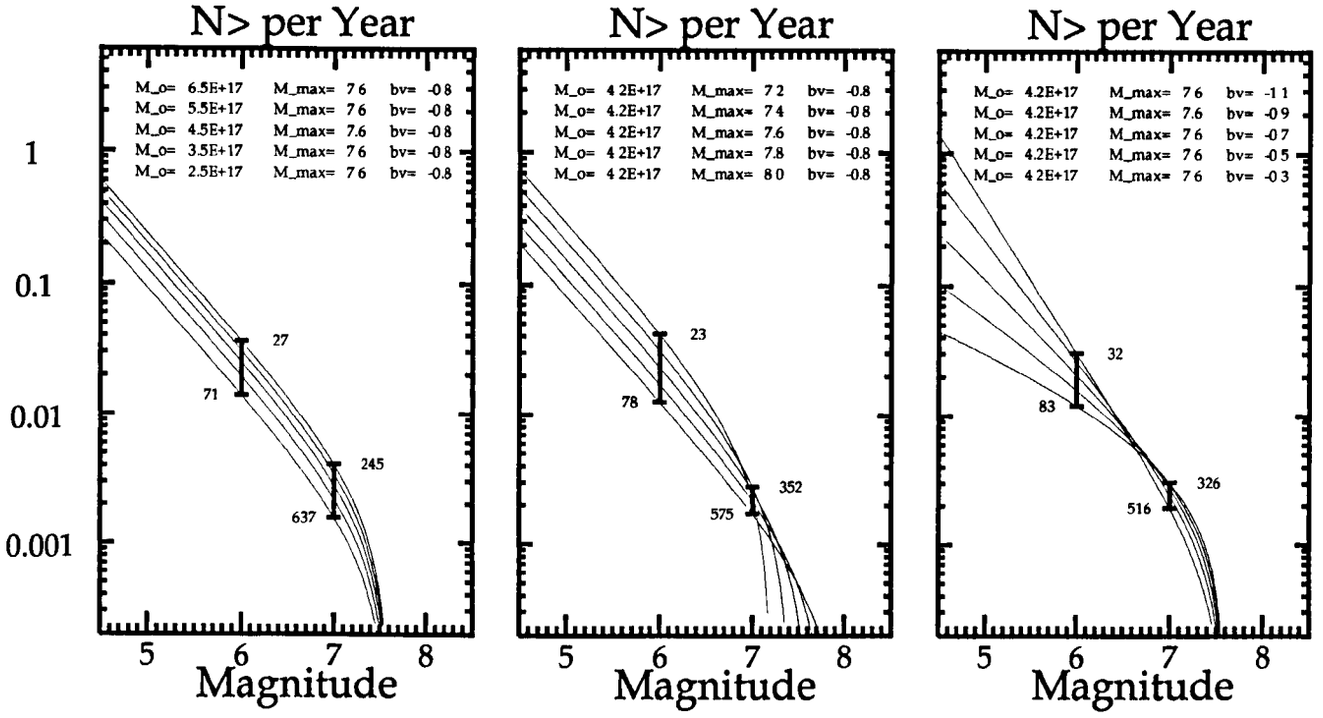

Figure 14. Estimated earthquake recurrence interval for that part of the California Continental Borderland spanned by the GPS network shown in Fig. 13. The three diagrams graph recurrence intervals based on truncated Gutenberg–Richter distributions covering probable ranges of moment rate, *b*-value, and maximum earthquake magnitude (listed across the top). This exercise suggests that *M*6+ earthquakes could recur at 27–77 yr intervals, whereas *M*7+ quakes might be encountered at 307–576 yr periods.

indicate that between 1 and 4 mm yr^{-1} of compression and 4–7 mm yr^{-1} of strike slip and are absorbed in the California Continental Borderland. With the Palos Verdes Fault taking some 3 mm yr^{-1} from the budget, perhaps 1–4 mm yr^{-1} of strike slip could be present on a through-going San Clemente Fault. When translated into an annual moment-release rate using Kostrov's formula, GPS strains predict that between 2.5 and 4.9×10^{17} N m yr^{-1} of earthquake potential is available for the California Continental Borderland between San Diego and Santa Cruz Island. Distribution of this moment budget among various earthquake magnitudes is arguable, but we suggest that $M > 6$ quakes in the Borderland could recur between 27 and 77 yr and $M > 7$ quakes might be found every 307 to 516 yr.

Although we have no direct evidence, it is reasonable to suspect that some of the other structures in the California Continental Borderland, such as Thirtymile Bank, Fortymile Bank, Osborn Bank or San Nicholas Island, may have been generated by localized uplift from San Clemente Island-style blind thrusts of various configurations. Further investigations employing 'geological geodesy' may help to localize some of these discrete faults within the broad compressional strain field detected by space geodesy.

ACKNOWLEDGMENTS

We thank Bob Bohannon for making available his seismic reflection data. This work was partially supported by Southern California Earthquake Center Award 662703 and National Science Foundation Grant EAR-9404962. Contribution 294 of the Institute of Tectonics, University of California, Santa Cruz CA, 95064.

REFERENCES

Allen, C.R., Silver, L.T. & Stehli, F.G., 1960. Agua Blanca fault—a major transverse structure of northern Baja California, Mexico, *Geol. Soc. Am. Bull.*, **71**, 457–482.

Anderson, J.G., 1979. Estimating the seismicity from geological structures for seismic-risk studies, *Bull. seism. Soc. Am.*, **69**, 135–158.

Bard, E., Hamelin, B. & Fairbanks, R.G., 1990. U-Th ages obtained by mass spectrometry in corals from Barbados: sea level during the past 130 000 years, *Nature*, **346**, 456–458.

Blake, M.C., Jr, Campbell, R.H., Dibblee, T.W., Jr, Howell, D.G., Nilsen, T.H., Normark, W.R., Vedder, J.G. & Silver, E.A., 1978. Neogene basin formation in relation to plate-tectonic evolution of San Andreas fault system, California, *Am. Assoc. Petrol. Geol. Bull.*, **62**, 344–372.

Bohannon, R.G. & Geist, E., 1996. Upper crustal structure and neogene tectonic development of the California Continental Borderland, *Tectonics*, submitted.

Chappell, J.M. & Shackleton, N.J., 1986. Oxygen isotopes and sea level, *Nature*, **324**, 137–140.

Crouch, J.K., 1981. Northwest margin of California Continental Borderland: marine geology and tectonic evolution, *Am. Assoc. Petrol. Geol. Bull.*, **65**, 191–218.

Crowell, J.C., 1979. The San Andreas fault system through time, *J. geol. Soc. Lond.*, **136**, 293–302.

Demets, C., Gordon, R.G., Argus, D.F. & Stein, S., 1990. Current plate motions, *Geophys. J. Int.*, **101**, 425–478.

Emery, K.O., 1958. Shallow submerged terraces of southern California, *Bull. geol. Soc. Am.*, **69**, 39–60.

Emery, K.O., 1960. *The sea off Southern California*, Wiley & Sons, New York.

Feigl, K. *et al.*, 1993. Space geodetic measurements of crustal deformation in central and southern California, *J. geophys. Res.*, **98**, 21 677–21 712.

Harrison, J.C., von Huene, R.E. & Corbatò, C.E., 1966. Bouguer

gravity anomalies and magnetic anomalies off the coast of southern California, *J. geophys. Res.*, **71**, 4921–4941.

Hummon, C., Schneider, C.L., Yeats, R.S., Dolan, J.F., Sieh, K.E. & Huftile, G.J., 1994. Wilshire fault: earthquakes in Hollywood?, *Geology*, **22**, 291–294.

Lajoie, K.R., 1986. Coastal tectonics, in *Active Tectonics, Studies in Geophysics*, pp. 95–124, National Academy Press, Washington DC.

Lajoie, K.R., Ponti, D.J., Powell, II, C.L., Mathieson, S.A. & Sarna-Wojcicki, A.M., 1991. Emergent marine strandlines and associated sediments, coastal California: a record of Quaternary sea-level fluctuations, vertical tectonic movements, climate changes, and coastal processes, in *Quaternary Non-glacial Geology: Coterminous United States: Geological Society of America Decade of North America Geology*, ed. Morrison, R.B., vol. K-2, 190–214.

Larson, K.M., 1993. Application of the Global Positioning system to crustal deformation measurements, 3, result from the southern California Borderlands, *J. geophys. Res.*, **98**, 21 713–21 726.

Lawson, A.C., 1893. The post-Pliocene diastrophism of the coast of southern California, University of California, *Dept of Geology Bull.*, **1–4**, 115–160.

Legg, M.R., 1991. Developments in understanding the tectonic evolution of the California Continental Borderland, in *From Shoreline to Abyss, SEPM Spec. Publ.*, **46**, 291–312.

Legg, M.R. & Kennedy, M.P., 1991. Oblique divergence and convergence in the California Continental Borderland, in *Environmental perils—SanDiego region*, eds Abbott, P.L. & Elliott, W.J., Guidebook for 1991 Geol. Soc. Am. Ann. Mtg, San Diego Assoc. of Geologists.

Legg, M.R., Luyendyk, B.P., Mammerickx, J., De Moustier, C. & Tyce, R.C., 1989. Sea beam survey of an active strike slip fault: the San Clemente fault in the California Continental Borderland, *J. geophys. Res.*, **94**, 1727–1744.

Lipps, J.H., 1967. Age and environment of a marine terrace fauna, San Clemente Island, California, *The Veliger*, **9**, 388–398.

Luyendyk, B.P., Kamerling, M.J., Terres, M.J. & Hornafius, J.S., 1985. Simple shear of southern California during Neogene time suggested by paleomagnetic declinations, *J. geophys. Res.*, **90**, 12 454–12 466.

Matsu'ura, M., Tanimoto, T. & Iwasaki, T., 1981. Quasi-static displacements due to faulting in a layered halfspace with an intervenient viscoelastic layer, *J. Phys. Earth*, **29**, 23–54.

McNeilan, T.W., Rockwell, T.R. & Resnick, G.S., 1996. Sense and rate of Holocene slip, Palos Verdes fault, southern California, *J. geophys. Res.*, **101**, 8317–8334.

Merifield, P.M., Lamar, D.L. & Stout, M.L., 1971. Geology of central San Clemente Island, California, *Geol. Soc. Am. Bull.*, **82**, 1989–1994.

Minster, J.B. & Jordan, T.H., 1987. Vector constraints on western U.S. deformation from space geodesy, neotectonics and plate motions, *J. geophys. Res.*, **92**, 4798–4804.

Moore, D.G., 1969. Reflection profiling studies of the California Continental Borderland: structure and Quaternary turbidite basins, *Geol. Soc. Am. Spec. Paper*, **107**, 142 pp.

Muhs, D.R., 1979. Marine terrace assignments, uplift rates and sea level events on San Clemente Island, California, *Geol. Soc. Am. Abstracts with Programs, Northeastern Section*, **11 (1)**, 484.

Muhs, D.R., 1980. Quaternary stratigraphy and soil development, San Clemente Island, California, *PhD thesis*, University of Colorado, Boulder, CO.

Muhs, D.R., 1983. Quaternary sea-level events on northern San Clemente Island, California, *Quat. Res.*, **20**, 322–341.

Muhs, D.R. & Szabo, B.J., 1982. Uranium-series age of the Eel Point terrace, San Clemente Island, California, *Geology*, **10**, 23–26.

Muhs, D.R., Kennedy, G.L. & Rockwell, T.K., 1994. Uranium-series ages of marine terrace corals from the Pacific coast of North America and implications for last-interglacial sea level history, *Quat. Res.*, **42**, 72–87.

Olmsted, F.H., 1958. Geologic reconnaissance of San Clemente Island, California, *US Geol. Surv. Bull.*, **1071-B**, 54–68.

Ridlon, J.B., 1972. Pleistocene–Holocene deformation of the San Clemente Island crustal block, California, *Bull. Geol. Soc. Am.*, **83**, 1831–1844.

Shepard, F.P. & Emery, K.O., 1941. Submarine topography off the California coast: canyons and tectonic interpretation, *Geol. Soc. Am. Spec. Paper*, **41**, 1–171.

Smith, W.S.T., 1897. A geological sketch of San Clemente Island, *US Geol. Surv. XVIII Ann. Rep.*, Part II, 461–496.

Stadum, C.J. & Susuki, T., 1976. The discovery of marine Pliocene strata on San Clemente Island, California, *Geol. Soc. Am. Abstracts with Programs, Cordilleran Section*, **8 (3)**, 411.

Stein, R.S., King, G.C.P. & Rundle, J.B., 1988. The growth of geological structures by repeated earthquakes: 2, field examples of continental dip-slip faults, *J. geophys. Res.*, **93**, 13 319–13 331.

Valensise, G., 1994. Geologic assessment of the relative contribution of strike-slip faulting, reverse-slip faulting and bulk squeezing in the creation of the Central Santa Cruz Mountains, California, *US Geol. Survey Professional Paper*, **1550F**, 23–47.

Valensise, G. & Ward, S.N., 1991. Long-term uplift of the Santa Cruz coastline in response in repeated earthquakes along the San Andreas fault, *Bull. seism. Soc. Am.*, **81**, 1694–1704.

Ward, S.N., 1986. A note on the surface volume change of shallow earthquakes, *Geophys. J. R. astr. Soc.*, **85**, 461–466.

Ward, S.N., 1990. Pacific–North America plate motions: new results from Very Long Baseline Interferometry, *J. geophys. Res.*, **95**, 21 965–21 982.

Ward, S.N., 1994. A multidisciplinary approach to seismic hazard in southern California, *Bull. seism. Soc. Am.*, **84**, 1293–1309.

Ward, S.N. & Valensise, G., 1994. The Palos Verdes terraces, California: bathtub rings from a buried reverse fault, *J. geophys. Res.*, **99**, 4485–4494.

Weldon, R.J. & Humphreys, E.D., 1986. A kinematic model of southern California, *Tectonics*, **5**, 33–48.

APPENDIX A: RECONSTRUCTION OF TERRACE INNER EDGES

A1 Terrace identification

The first step in our reconstruction of the marine terraces of San Clemente Island identifies terrace 'inner-edge' fragments (the intersection of each wave-cut platform and the cliff that backs it) from 1 : 24 000 scale US Geological Survey 7.5 minute quadrangles. Terrace inner edges are identified from the contrast in contour density between the relatively level wave-cut platform and its backing cliff, typically some 10 to 20 m in height. One complication in terrace identification is sedimentary cover. The younger wave-cut platforms are generally topped by a veneer of marine sediments (≤ 2 m) deposited at the time of terrace carving; however, a significantly thicker coat of intervening alluvial sediments may hide the inner edge of older terraces. Once identified, terrace inner-edge locations and elevations are noted. We estimate that the elevations have errors of about ± 10 m.

A2 Terrace correlation

The next step attempts to correlate the identified terrace inner-edge fragments with a particular strandline. To label the strandlines we used Muhs' (1980) nomenclature for terraces 1 to 10, bottom to top (younger to older), and, numbered 11 to 14, four other well-expressed terraces outside Muhs' study area. Taking representative transects perpendicular to the island's southwest flank 2 km northwest of Eel Point and 3 km northwest of China Point (Fig. 4), all 14 terraces could be paired with identified inner edges. Because the terraces are

nearly level, we were then able to continue the correlation around parts of the island not mapped by Muhs simply by extending sideways each inner edge following the associated break in slope.

In addition to the 14 main terraces, each previous investigator has reported as many as a half-dozen more subdued terraces. These secondary terraces (which we list using the number of the immediately lower terrace and the suffix a, b, c) may have been created by 'weak' highstands having either a short duration or a low formation elevation. Of special interest for the reconstruction of sea-level during the last major interglacial are the low-elevation terrace remnants between 4 and 24 m. Those around Wilson Cove and between West Cove and Eel Point are too scattered to warrant firm interpretation, and suspicion exists that they have been altered by intervening faulting. The 25 ft (7.5 m) contour interval on the 1:24 000 scale quadrangles was too coarse to reconstruct the 5 m terrace that Muhs (1980) mapped as Terrace 1 between the Northwest Harbor and Eel Point, but we did include it in the discussion on dating the terrace sequence.

Our reconstruction began with Terrace 2, which is the best expressed geomorphically and can be followed for nearly 40 km from Northwest Cove to Pyramid Cove. Terraces 3 to 7 also extend for nearly the entire length of the island with a variable degree of clarity. Starting with Terrace 8, the palaeoshorelines begin retreating towards the southern end of the island, indicating that the northernmost 8–10 km of San Clemente Island emerged more recently than its wider and higher middle and southern portions. An interesting feature of Terrace 8 is its bottleneck northern end (Fig. 8). This terrace section encircles a localized high for the northern half of the island, and may reflect the coalescence of two pieces of land separated by a $\sim$50 m deep sound. Taken along their longer axis, terraces 12 and 13 are almost symmetrical with respect to the highest point on the island (601 m), suggesting that this was the first land to emerge. By analogy, the peak encircled by the northern tip of Terrace 8 may represent a secondary centre of uplift. All of the terraces are asymmetrical relative to the island's width. The few terrace remnants preserved on the northeastern flank of the island define rectilinear palaeoshorelines similar to the modern coast, whereas the terraces on the opposite flank describe an outward convex arch culminating halfway between Lost Point and China Point. Lawson's '1500 ft terrace', the highest of the identified terraces is very discontinuous and not resolvable from the available maps. We simply mapped this terrace along the 1500 ft contour (458 m).

A3 Terrace deformation

An important element of terrace reconstruction is an assessment of the extent to which terrace surfaces have been deformed after they have been cut. With two exceptions, all of the terraces tend to run parallel to each other and to the modern shoreline, and size and shape differences between younger and older terraces are progressive rather than abrupt. Nearly all of the palaeoshorelines trend smoothly for the entire length of the terraced portion of the island, and drainages appear to have always developed perpendicular to the existing shoreline.

Exception 1. Near the northern end of the island, terrace inner edges 2 to 7 distort in a left-stepped kink along the alignment between Wilson and West coves (Fig. 4). This alignment marks also the boundary across which the northern tip of the island seems to have been offset westwards. The left-lateral strike-slip fault needed to accomplish this motion has, however, never been described by field investigators. Probably, this offset is only an apparent one, and the strandlines were laid out on a fault-related but pre-existing kink.

Exception 2. More serious deformations occur about 2 km northwest of China Point, where both the modern shoreline and the inner edge of Terrace 2 are indented as they cross the N10°E-striking normal faults mapped by Olmsted (1958). These faults share a west-side up sense of motion, yet they seem to offset the terraces left-laterally. This phenomenon has two explanations: the faults cut a sloping topography, producing an apparent lateral throw of the terrace surface in map view; and/or the faults accelerate or decelerate the local rate of uplift which increases or decreases the rate of coastal advancement on the footwall and hanging wall. The second explanation requires that the faults be active during the carving of Terrace 2 (Late Pleistocene). The first explanation remains valid even if the faults became inactive before the carving of Terrace 2. The absence of detectable vertical displacement of the younger terraces tells us that most displacement on these normal faults occurred prior to Late Pleistocene, or else that their slip rate has always been minimal. Rates faster than 0.1 mm yr^{-1} on a fault cutting a 100 ka terrace (approximate age of Terrace 2) would produce 10 m of vertical displacement and would be visible in the geological record, even at our level of resolution.

Secondary faults played a significant role during pre-Late Pleistocene time in shaping San Clemente Island even prior to its emergence. Evidence indicates that some of these faults, certainly those near Pyramid Cove, experienced several hundred metres of total slip. Still, by and large, we believe that the rates and wavelengths of deformation produced by any of the surficial faults on San Clemente Island are an order of magnitude smaller than those generated by the parent thrusts underlying the island's core anticline.

A4 Terrace dating/uplift rates

In comparison to terrace correlation, terrace dating leaves more room for uncertainty due to: (1) conflicts in the two uranium-series dates available (127 ± 7 ka and 111 ± 3 ka) from coral samples collected on Terrace 2; (2) uncertainties in inner-edge elevations of some key terraces; and (3) uncertainties in the formation elevation of recent highstands, particularly the 81 and 102 ka (substages 5a and 5c of the oxygen isotope record).

The two available dates for Terrace 2 lead to conflicting scenarios (see small arrows in Fig. 10)—the first age may relate to the 124 ka highstand (oxygen isotope stage 5e) when sea-level stood at 6 m above today's level; the second age falls on a relative lowstand between the 124 and the 102 ka highstands, when sea-level stood 60 to 80 m below the present level. A conservative treatment of the uncertainty in direct age determinations limits the origin of Terrace 2 no more finely than to one of the stage-5 highstands: the 124 ka (formation elevation +6 m), the 102 ka (−7 m), or the 81 ka (−12 m). Taking Terrace 2 at 32 m elevation, these choices yield rates of uplift of 0.21, 0.38 and 0.54 mm yr^{-1}.

For an uplift rate of 0.5 mm yr^{-1}, each metre of uncertainty in inner-edge elevation translates to a 2000 yr uncertainty in terrace age. Given the 7.5 m contour interval of the maps that we used in the reconstruction and an unknown few metres of terrace cover, our ± 10 m elevation uncertainty yields age uncertainties of $\pm 20\,000$ years, about the same variation as for the direct dating.

Uncertainties arising from unknown formation elevations work the same way as uncertainties in inner-edge elevations, and they can be large, even dominant, if uplift is slower than 0.5 mm yr^{-1}. For example, a 0.3 mm yr^{-1} uplift rate should raise a 81 ka terrace by 24 m; however, because the 81 ka highstand elevation is uncertain between -20 and -5 m relative to modern sea-level (e.g. Bard, Hamelin & Fairbanks 1990; Lajoie *et al.* 1991; Muhs *et al.* 1994), the terrace might be found anywhere from 4 to 19 m elevation. With the vertical spacing of the lower terraces of San Clemente Island being roughly 10 m (see Table 1), uncertainties in inner-edge elevation could make two or three terraces candidates for the 91 ka highstand.

To minimize ambiguities arising from direct dating of individual fossil samples or to constrain terrace ages in the absence of datable fossils, it is helpful to correlate a full set of observed terrace inner-edge elevations with reconstructed global sea-level histories. The procedure, originally formalized by Lajoie (1986), was introduced in Fig. 10. For simplicity, the calculations assume constancy of the rate of uplift and do not take into account the fact that higher terraces occurring closer to the centre of uplift should record slightly (<10 per cent) faster rates. Terrace surfaces along an idealized transect perpendicular to the southwestern flank of the island were assigned Muhs & Szabo's (1982) average elevations (Table 1). To reduce the number of possible correlations, we keyed on the 124 ka highstand. Assuming that terraces 2 (32 m), 3 (40–53 m) and 4 (55–68 m) were created by this highstand, rates of uplift would be 0.21, 0.27–0.38 (average 0.33) and 0.40–0.50 (average 0.45) mm yr^{-1}, respectively. All three options match some terraces and miss others: (1) the slowest rate (0.21 mm yr^{-1}) misses completely Terrace 3, and implies the existence of an unseen 102 ka strandline slightly above 10 m elevation; (2) a rate of 0.33 mm yr^{-1} misses Terrace 5, one of the best-expressed terraces of San Clemente Island, and does not explain Terrace 1 at 5 m; (3) a rate of 0.45 mm yr^{-1} provides a good fit to the lower terraces, particularly if the formation elevations of the 81 and 102 ka highstands were somewhat lower than presumed, but completely misses terraces 3 and 6. Under this assumption, Terrace 1 at 5 m could have been created by one of the highest peaks of stage 3, for instance at 65 ka when the sea is assumed to have stood at about -30 m relative to its modern level (Chappell & Shackleton 1986).

Considering that Terrace 2, the island's best-expressed geomorphic surface, was presumably formed during a major highstand and that the dated corals are indicative of climatic conditions comparable to or warmer than today's (hence the likelihood that its highstand had a positive formation elevation), we are prompted to favour a 124 ka age.